Unveiling the odor representation in the inner brain of *Drosophila* through compressed sensing

Kiri Choi ⬤,* Won Kyu Kim ⬤, and Changbong Hyeon ⬤†

School of Computational Sciences, Korea Institute for Advanced Study, Seoul 02455, Korea

The olfaction begins when odorant molecules stimulate a finite number of receptor types in the olfactory neurons. According to the recent connectomics data of the *Drosophila* olfactory system, the olfactory neural circuit is multilayered and there is an overall dimensionality reduction from the input to output layer. Compressed sensing (CS) is an algorithm that enables the recovery of high-dimensional signals from the data compressed in a lower dimension when the representation of such signals is sufficiently sparse. By analyzing the recent *Drosophila* connectomics data, we find that the organization of the *Drosophila* olfactory system effectively satisfies the necessary conditions for CS to work. The neural activity profile of projection neurons (PNs) can be faithfully recovered from a low-dimensional response profile of mushroom body output neurons (MBONs), which can be reconstructed using the electrophysiological recordings of a wide range of odorants. By leveraging the residuals calculated between the measured and the predicted MBON responses, we visualize the perceptual odor space using the residual spectrum and discuss the differentiability of an odor from others. Our study highlights the sparse coding of odor to the receptor space as an essential component for odor identifiability, clarifying the principles underlying the concentration-dependent odor percept. Further, simultaneous exposure of the olfactory system to many different odorants saturates the neural activity profile of PNs, significantly degrading the capacity of signal recovery and resulting in a perceptual state analogous to "olfactory white." Our study applying CS to the real connectomics data encompassing the neural circuitry from PNs to MBONs via Kenyon cells provides quantitative insights into the neural signal processing and odor representation in the inner brain of *Drosophila*.

I. INTRODUCTION

Olfaction is a sensory process of detecting chemical stimuli in the environment. Despite its fundamental importance, still left ambiguous are basic quantities associated with the understanding of olfaction, such as the number of differentiable odors and odor percepts [1–3]. While there have been attempts to study the representation of odorants or odor [4,5], its translation to odor differentiability is not entirely clear. Further, odor identification and perception are deemed highly subjective and context dependent, varying from one individual to another [6]. This is in stark contrast to other sensory processes such as vision, which is quantitatively understood as the combined responses of distinct types of photoreceptors to

visual signals continuous in the spectral domain. However, the conditions for understanding the insect olfactory system have greatly been improved in recent years, thanks to the three-dimensional map of neuronal morphology and the synaptic connectivity reconstructed from high-resolution electron microscopy (EM) images, such as *Drosophila* hemibrain data set [7], the olfaction-specific FAFB data set [8], and more recently the full connectome of the *Drosophila* larva [9]. By making the neural circuitry of the insect brain accessible at synapse resolution, these connectomics data sets open a new avenue to a quantitative understanding of the principles behind olfactory processing.

As illustrated in Fig. 1(a), olfactory signaling starts when an odorant binds to olfactory receptors (ORs) in the olfactory receptor neurons (ORNs). Each ORN expresses a specific type of OR, exhibiting homotype-dependent responses to input odorants. The same type of ORN converges to a particular set of uniglomerular PNs (uPNs) forming a glomerulus in the antennal lobe (AL) [10]. The signals converged and sorted at uPNs transfer to the higher olfactory centers such as the mushroom body (MB) calyx and the lateral horn (LH), where synaptic wirings with higher order neurons integrate the signal. Specifically, in the MB calyx, extensive and seemingly randomized signal integration is made at the synaptic interface between PNs and the Kenyon cells (KCs) [11,12], which passes over to mushroom body output neurons (MBONs) whose dimension is smaller than that of PNs. In LH, the compartmentalized spatial organization of PNs translates to

---

*Present address: Department of Molecular, Cellular and Developmental Biology, Yale University, New Haven, CT 06511, USA; Quantitative Biology Institute, Yale University, New Haven, CT 06511, USA; Swartz Foundation for Theoretical Neuroscience, Yale University, New Haven, CT 06511, USA; Contact author: kiri.choi@yale.edu
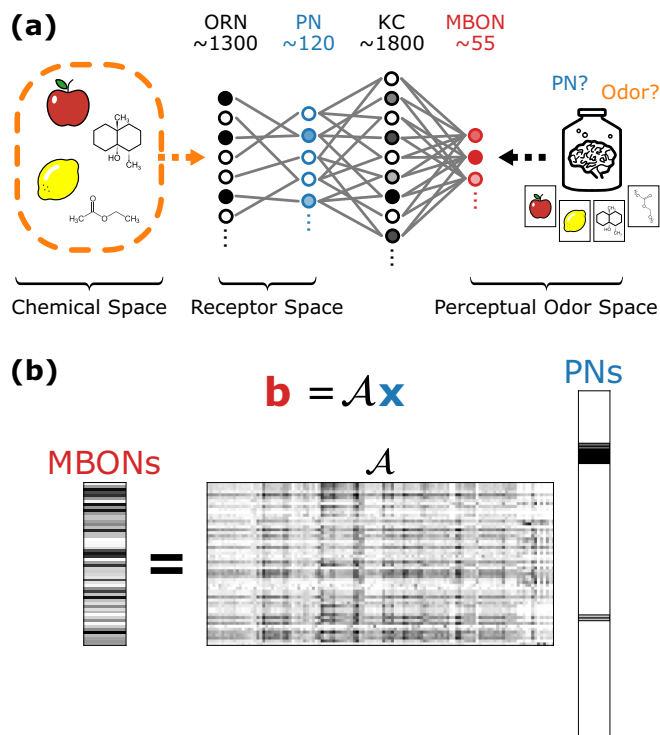
†Contact author: hyeoncb@kias.re.kr

FIG. 1. Olfactory processes in *Drosophila*. (a) An odor represented in the chemical space is encoded by a sparse set of ORs/PNs in the receptor space. Highly integrated olfactory signals in the perceptual odor space are deciphered at higher cortical areas, which infers the activity profiles of uPNs (blue) and hence the olfactory code from the relatively low-dimensional and randomized information integrated into MBONs (red). (b) Our problem is formulated to solve for *n*-dimensional sparse olfactory codes (**x**) encoded by PNs from a set of underdetermined linear equations in the form of $\mathbf{b} = \mathcal{A}\mathbf{x}$, where **b** and $\mathcal{A}$ represent the $m(< n)$-dimensional response profile of MBONs and the $m \times n$ sensing matrix, respectively.
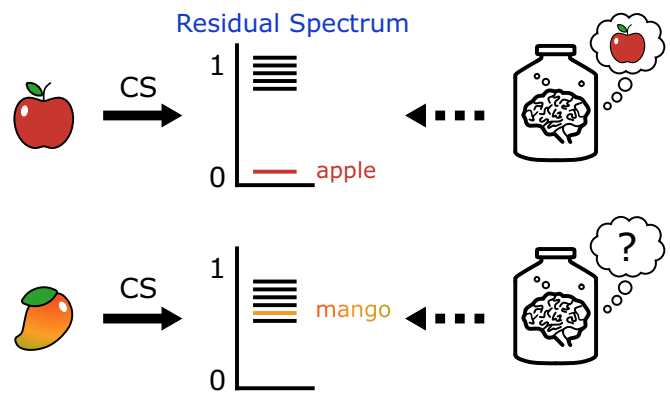

FIG. 2. Odor representation and perceptual odor space. A putative structure of the perceptual odor space. The gap between the self-residual and cross residuals in the residual spectrum decides the differentiability of a given odor from others. In the illustration, the apple odor is highly differentiable from others, but the mango odor is not.

a more stereotyped signal integration by lateral horn neurons (LHNs) [13–16].

Previous studies have demonstrated that, in the *Drosophila* olfactory system, the downstream components of KCs such as MBONs and dopaminergic neurons (DANs) are responsible for encoding the hedonic valence and value [17,18]. However, given the apparent compression of neural information in MBONs, it is of great interest to explore whether higher cortical areas can decipher a neural activity of MBONs in response to the odor encoded into the neural activity profile in uPNs and determine the odor identity utilizing a neural process analogous to solving a constrained optimization problem [12,19–23] [Fig. 1(a)]. Among several candidate algorithms, compressed sensing (CS), which determines the sparsest solution of a set of underdetermined linear equations, has previously been applied to the *Drosophila* olfactory system as a means to identify the chemical composition of an odor from activity profiles (i.e., neuronal firing rates) of ORNs, PNs, or KCs [21,24–27]. Provided that the chemical composition of an odor is sparsely represented in the chemical feature space [28,29], CS can reliably uncover the odor identity. CS has been applied to the olfactory sensing in the scope of the odorant-OR interface [21,26,27] and between odorants and

KCs [23,25]. The previous studies using CS on olfaction have offered valuable insights into the odor codes and odor identification process; yet, their discussions were largely limited to the relationship between the chemical feature space and the receptor space.

In this study, aside from the odor valence information in MBON, we analyze the electrophysiological responses on the neural circuit of the *Drosophila* olfactory system revealed from the connectomics data, so as to investigate (i) whether CS can accurately reconstruct the odor code from the highly integrated and compressed MBON response profile and (ii) whether the perception of a given odorant(s) is unambiguously discernible from other odors in the perceptual odor space (Fig. 1). We test the capacity of CS in recovering uPN activities from MBON response profiles by reconstructing the latter based on the electrophysiological recordings of neural spiking activities [29,30]. More specifically, we calculate the spectrum of residuals to visualize the perceptual odor space by comparing the reconstructed odor response profiles to those projected onto other olfactory stimuli (see Fig. 2). Exploring how the perceptual odor space changes when multiple odorants are mixed, our study demonstrates that the simultaneous introduction of diverse odorants significantly deteriorates the capacity of CS, an observation in line with the notion of "olfactory white." We show that a significant variation in concentration can yield a large deviation in the odor code and alter the extent of odor identifiability. By employing the CS algorithm as a means to probe the olfactory processing in the inner brain of *Drosophila*, our study offers insights into how odor perception is realized, while demonstrating the functional benefits of randomized wiring and sparse coding.

II. DATA PREPARATION

The connectomics data analyzed in this study is based on the hemibrain data set (hemibrain v1.2.1) [7]. When querying the neurons, we chose only PNs, KCs, and MBONs that exhibit at least one synaptic connection. We then collected a total of 119 uPNs synapsing with 1776 KCs, which in turn synapse

with 56 MBONs expressing 34 MBON types that project to MB in the right hemisphere. As for the glomerular labels, we used the one supplied by the hemibrain data set. In case a uPN was associated with multiple glomeruli, we referred to the labeling from the FAFB data set [8], which provided their version of the glomerular label, along with the corresponding neuron ID in the hemibrain data set. Additionally, we updated several labels following the recent community agreement to rename three glomeruli with conflicting glomerulus labels to amend the homotypes VC3l, VC3m, and VC5 to VC3, VC5, and VM6, respectively [31]. In this study, we designate the homotype of a PN by the glomerulus innervated by the dendrites, so that the homotype is uniquely defined for uPNs.

The odor response profile was reconstructed by merging two different data sets that measured the electrophysiological responses to the exposure of an odorant [29,30]. The experimental procedure used several different concentrations of odorants. 10^{-2} volume per volume (v/v) dilution with either H_2O, paraffin oil, or mineral oil is used, except for geosmin which used 10^{-3} dilution. We explicitly stated the dilution level whenever a different odorant concentration was used. When there was an overlap between the data sets, we selected the more recent recordings by Seki *et al.* [30]. The connection between ORs and the respective glomerulus is identified through a literature search [32–35]. The data set by Hallem *et al.* contained a recording corresponding to Or33b. Homotype DM3 coexpresses Or33b and Or47b, while homotype DM5 coexpresses Or33b and Or85a [33], which we incorporated manually by adjusting the odor response profile. When testing naturalistic inputs, we only chose odorants that elicited a strong response ($\geqslant 40$) to at least a single recorded homotype. This criterion resulted in odor response profiles for 39 homotypes against 96 distinct odorants (+baseline firing rate). A keen reader might notice that neither of the data sets was comprehensive enough to cover all 58 homotypes available in the hemibrain data set. For any missing measurements, we assumed no response and assigned zero values.

The functional group information was taken from Hallem *et al.* [29], while the odor valence information was acquired from the literature [8,36–39].

III. ALGORITHM OF COMPRESSED SENSING

Since its original inception by a group of mathematicians and engineers [40,41], CS has garnered substantial interest due to the apparent overcoming of the Shannon-Nyquist sampling theorem [42,43], leading to its application in many different areas [44–46]. For a compressible signal that can be mapped to a sparse representation, CS is employed to recover the original signal by solving for the sparsest solution of a set of underdetermined linear equations. The first set of applications focuses on minimizing the quantity of measured input when the measurement process is expensive. Another set of applications recognizes the implementation of sparse representation for a high-dimensional signal. The primary example would be various attempts at analyzing the signal processing inside a brain. The brain has been suggested to benefit from utilizing CS as a means to reduce the bandwidth and storage necessary for neural processes, including vision [47], olfaction [12,21,24–27], and others [48,49], thus

inferring high-dimensional signals from low-dimensional sensory input [50,51].

Consider a set of linear equations

$$\mathbf{b} = \mathcal{A}\mathbf{x}, \tag{1}$$

where $\mathbf{x}$ is an unknown n-dimensional vector, and $\mathbf{b}$ and $\mathcal{A}$ are the preassigned m-dimensional vector and $m \times n$ matrix, respectively. If our goal is to find $\mathbf{x}$ that satisfies the equation for given $\mathbf{b}$ and $\mathcal{A}$, the problem is trivial when the dimension of $\mathbf{b}$ is larger than the dimension of $\mathbf{x}$ ($m \geqslant n$). However, when $m < n$, this is an underdetermined (overparametrized) problem, allowing infinitely many solutions for $\mathbf{x}$. If our interest is to find $\hat{\mathbf{x}}$, the sparsest solution of $\mathbf{x}$ subject to Eq. (1) such that the vector $\mathbf{x}$ has the smallest number of nonzero values, our problem becomes

$$\hat{\mathbf{x}} = \arg\min_{\mathbf{x}} \|\mathbf{x}\|_0 \quad \text{subject to } \mathbf{b} = \mathcal{A}\mathbf{x}, \tag{2}$$

where $\| \cdot \|_0$ is the cardinality or the l_0 pseudonorm that counts the nonzero elements in a vector such that $\|\mathbf{x}\|_0 = K$ is the sparsity of the vector $\mathbf{x}$. However, minimizing the cardinality of $\mathbf{x}$ under a constraint corresponds to a nonconvex optimization problem, which is computationally demanding. CS modifies Eq. (2) by considering an l_1-norm minimization instead, which algorithmically simplifies Eq. (2) to a convex optimization problem:

$$\hat{\mathbf{x}} = \arg\min_{\mathbf{x}} \|\mathbf{x}\|_1 \quad \text{subject to } \mathbf{b} = \mathcal{A}\mathbf{x}, \tag{3}$$

where $\|\mathbf{x}\|_1 = \sum_{i=1}^{n} |x_i|$. If the following two conditions are met, the solution of Eq. (3) is identical to that of Eq. (2), allowing one to recover the sparsest solution $\hat{\mathbf{x}}$ with a high probability [40,43]. First, as the general rule of thumb, the dimension of $\mathbf{b}$ should asymptotically be larger than the order of $O(K \log(n/K))$. Next, the sensing matrix $\mathcal{A}$ must be effectively *incoherent*, meaning that randomly selected $2K$ column vectors must be uncorrelated to each other (see Appendix A).

We constructed the sensing matrix $\mathcal{A}$ by taking a product of the normalized synaptic connectivity matrices, $\mathcal{C}^{PN-KC}$ and $\mathcal{C}^{KC-MBON}$ (see Supplemental Material Fig. S1 [52]). That is, each column and row of $\mathcal{C}^{PN-KC}$ and $\mathcal{C}^{KC-MBON}$ is normalized, respectively. The l_1-norm minimization was performed to generate the solution $\hat{\mathbf{x}}^\alpha$ for a given MBON activity profile $\mathbf{b}^{\text{meas},\alpha}$ acquired from uPN expression to an odorant α. We used the Sequential Least SQuares Programming (SLSQP) optimizer implemented in the SCIPY package constrained to $\mathbf{b} = \mathcal{A}\mathbf{x}$ with unconstrained variable boundaries.

When assessing the capacity of CS in odor identification for an odorant α, we evaluate the similarity between $\mathbf{b}^{\text{meas},\alpha}$ and $\mathbf{b}^\alpha = \mathcal{A}\hat{\mathbf{x}}^\alpha$, where $\hat{\mathbf{x}}^\alpha$ is the solution of Eq. (3) (see Appendix B).

IV. CAPACITY OF COMPRESSED SENSING IN SIGNAL RECOVERY

We demonstrate that CS can reliably recover the uPN activity profile from the MBON response profile through the sensing matrix defined by the product of two synaptic connectivity matrices (Fig. S1 [52]). Consider a situation depicted in Fig. 1(a), where *Drosophila* whiffs the distinctive odor of an apple, in which the apple odor in the chemical space is

encoded into uPN activity profiles. Before an olfactory signal reaches the higher cortical area, the signal is integrated as it passes through higher-order olfactory neurons such as KCs and MBONs. Then, we ask whether or not the higher cortical area can infer a high-dimensional uPN activity from a low-dimensional MBON response profile and identify the odor code as an apple odor. It turns out that the perceptual differences between odors are not straightforward to conclude by simply comparing two response profiles compressed in MBONs represented in m-dimensional vectors (see the MBON profiles of methyl benzoate and ethyl benzoate in Fig. S2 [52], for instance, and the analysis given in Appendix C). Therefore, given the MBON response profile, we leverage CS to solve the inverse problem of finding the sparsest representation of the odor in uPN activities instead. Ideally, the MBON activity expected from the solution of CS processed through the sensing matrix should reproduce what was originally given. Furthermore, provided that the odor code of an apple is discernible from that of other odors, the odor representation of an apple at MBONs should be unique and clearly discernible from others.

In CS, an MBON response profile and a uPN activity profile are translated to the vectors $\mathbf{b}$ and $\mathbf{x}$, respectively. We build uPN activities ($\mathbf{x}^{\mathrm{meas},\alpha}$) from the electrophysiological recordings [29,30] for various odorants or odorant mixtures, designated by α, and calculate the corresponding MBON response profile via the relation $\mathbf{b}^{\mathrm{meas},\alpha} = \mathcal{A}\mathbf{x}^{\mathrm{meas},\alpha}$. CS uses $\mathbf{b}^{\mathrm{meas},\alpha}$ and $\mathcal{A}$ to determine the sparsest uPN representation for α ($\hat{\mathbf{x}}^\alpha$). We next calculate the "residual" denoted by $r_{\alpha|\beta}$ (see Appendix B for further detail), defined between the measurement ($\mathbf{b}^{\mathrm{meas},\alpha}$) and the calculation ($\mathcal{A}\hat{\mathbf{x}}^\alpha$) projected on itself [$\mathcal{A}\delta_\alpha(\hat{\mathbf{x}}^\alpha)$] or another odor [$\mathcal{A}\delta_\beta(\hat{\mathbf{x}}^\alpha)$] (Appendix B). The spectrum of residuals ($\{r_{\alpha|\beta}\}$), especially the gap between the self-residual ($r_{\alpha|\alpha}$) and the cross-residuals ($r_{\alpha|\beta}$, $\beta \neq \alpha$), provides an insight into the differentiability of the odor α in the perceptual odor space (Fig. 2). If the self-residual is small and well separated from all other cross-residuals ($r_{\alpha|\alpha} \ll r_{\alpha|\beta}$ for all $\beta \neq \alpha$), then the representation of odor α in the perceptual space is unique and easily discernible from others (Fig. 2, top). In contrast, if the self-residual is comparable to other cross-residuals ($r_{\alpha|\alpha} \simeq r_{\alpha|\beta}$), it is difficult to differentiate the odor α from other odors, implying that the perceptual odor space of α is not well isolated (Fig. 2, bottom). The spectrum of residuals $\{r_{\alpha|\beta}\}$ allows us to assess the specificity of the odor α among other odors, offering glimpses into the perceptual odor space.

Embracing the criterion by Seki *et al.*, who used either 30 spikes/s or 50 spikes/s as the detection threshold to demonstrate that a strong response to an odor is sparse [30], we define the strong response as the one evoking more than 40 spikes/s, analogous to the "winner takes all" (WTA) approach [23], and take into account only the odorants that elicit a strong response to at least one glomerular homotype in the experiments. The combined data set contains the recordings from 39 glomeruli, which correspond to ~80 uPNs (Fig. 3), in response to 96 different odorants encompassing diverse odor types that feature different functional groups and behavioral responses (see Supplemental Material Table S1 [52]). Here, we assume that the activation of neurons is linearly correlated with equal gain in response to the odorants [53] and that uPNs extending from the same glomerulus receive identical input
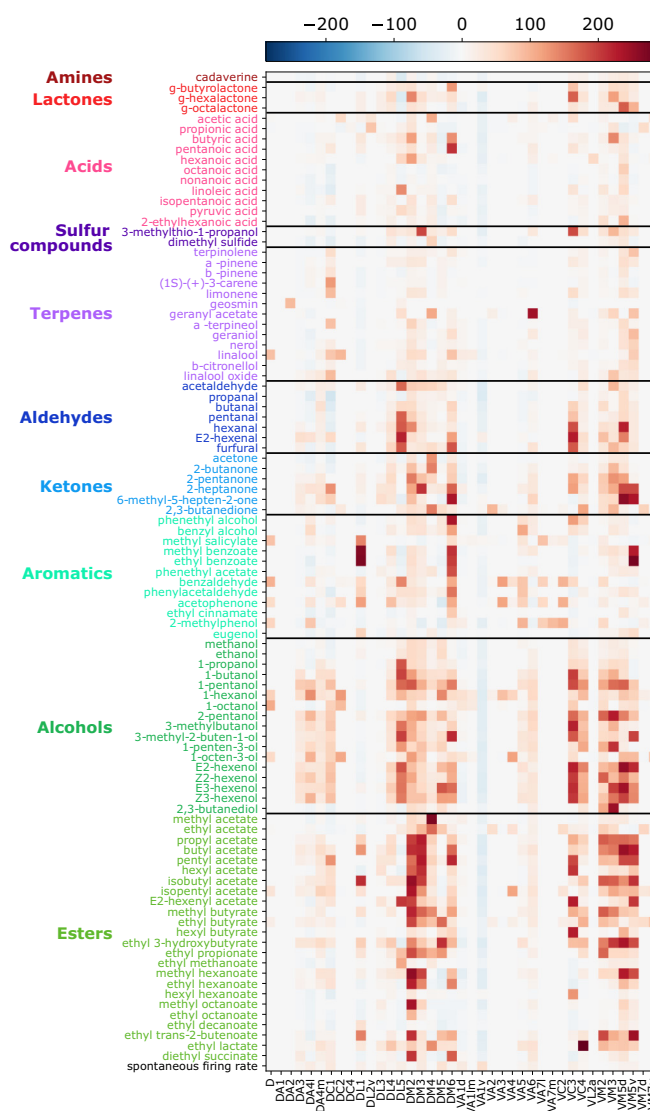

FIG. 3. uPN activity profiles sorted by odorant functional groups. The electrophysiological recordings of 39 homotypes to 96 odorants (+ basal response labeled as "spontaneous firing rate") where at least a single homotype exhibited a strong response (⩾40 spikes/s). The labels are color coded based on the same odor categorization used by Hallem *et al.* [29] (dark red: amines; red: lactones; pink: acids; purple: sulfur compounds; violet: terpenes; dark blue: aldehydes; blue: ketones; emerald: aromatics; green: alcohols; olive: esters).

(see Appendix D for the case of nonlinear filter). Furthermore, we also assume that ~40 uPNs out of 119 uPNs included in our circuit, which are not part of the measured 39 glomeruli, do not respond to the tested odorants.

Our CS framework correctly identifies 83 odorants out of 96 odorants (~86%), indicating that $\mathbf{b}^{\mathrm{meas},\alpha} \approx \mathcal{A}\hat{\mathbf{x}}^\alpha$ (and $\mathbf{x}^{\mathrm{meas},\alpha} \approx \hat{\mathbf{x}}^\alpha$), with $r_{\alpha|\alpha}$ being minimal among all the residuals ($\{r_{\alpha|\beta}\}$) (Fig. 4; see Supplemental Material Fig. S3 [52] for an alternative illustration of the result). The 13 odorants that failed in our test are either alcohols or esters, which include 1-butanol, 1-pentanol, 1-hexanol, 2-pentanol, 1-octen-3-ol, 3-methyl-2-buten-1-ol, trans-2-hexen-1-ol (E2-hexenol), cis-2-Hexen-1-ol (Z2-hexenol), trans-3-hexen-1-ol (E3-hexenol),
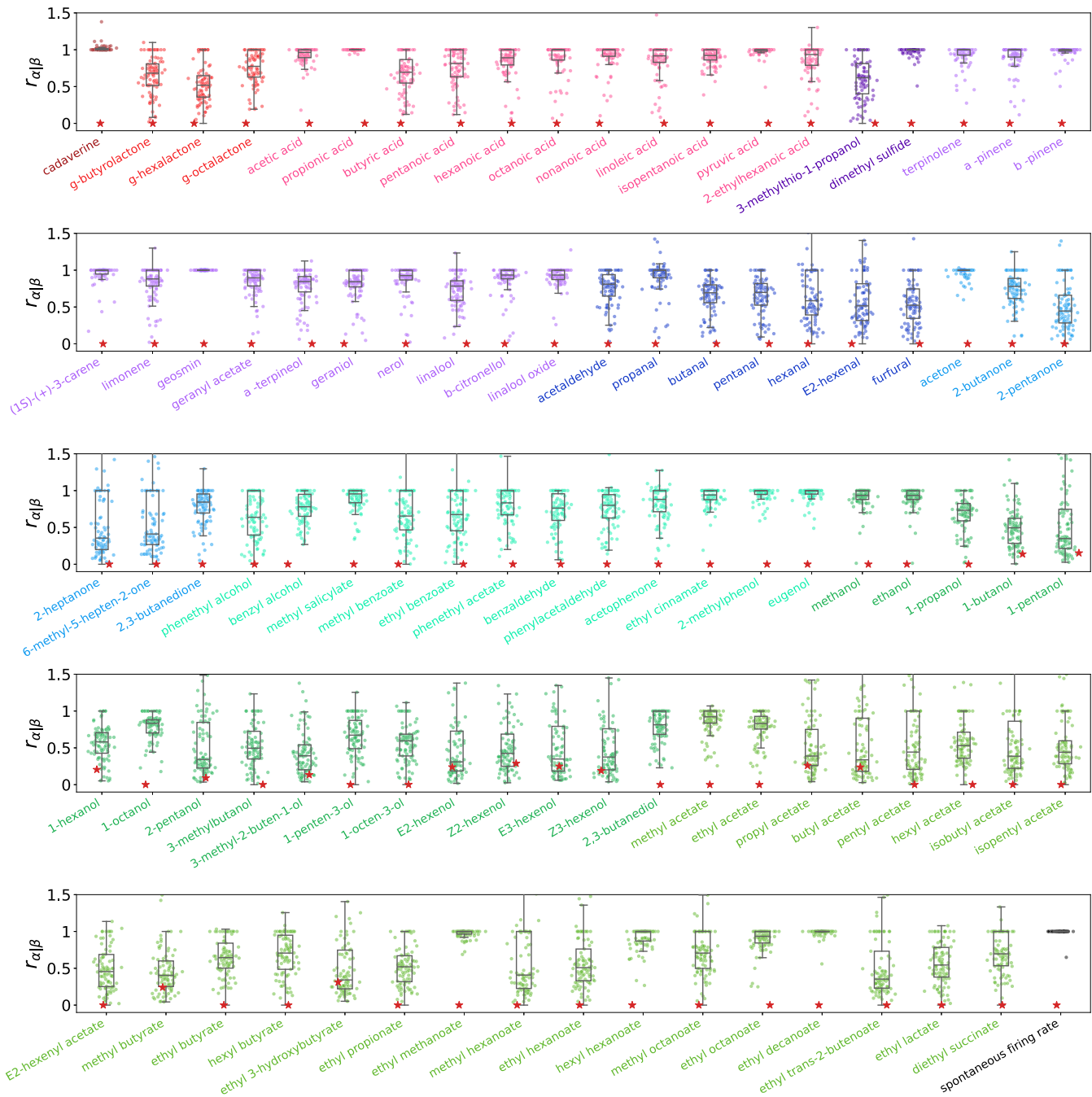
FIG. 4. Residual spectra, $\{r_{\alpha|\beta}\}$, calculated for 96 odorants. The residual $r_{\alpha|\beta}$ calculated for an input odorant α against other odorants β denoted in the horizontal axis. Red stars denote the self-residual $r_{\alpha|\alpha}$. The same color code as Fig. 3 is used.

cis-3-Hexen-1-ol (Z3-hexenol), propyl acetate, butyl acetate, and ethyl 3-hydroxybutyrate. For the statistical analysis of the residual spectrum for an odorant α ($\{r_{\alpha|\beta}\}$), we calculate the Z score of the self-residual ($r_{\alpha|\alpha}$) (see Appendix B). Many odorants exhibit significantly negative Z scores, indicative of a large gap between $r_{\alpha|\alpha}$ from $r_{\alpha|\beta}$ ($\beta \neq \alpha$) and a well-partitioned perceptual odor space for α [Fig. 5(a)]. We also study the performance of CS when the sensing matrix is replaced with various types of statistically random matrices (see Appendix E).

Successful identification of odorant α hinges on the sparsity (K) of its input uPN activity profiles $\mathbf{x}^{\text{meas},\alpha}$ [Fig. 5(b)].

An activity profile with a large K, which is found to correlate with the Z score [Fig. 5(c)], gives rise to a large self-residual ($r_{\alpha|\alpha}$) resulting in a Z score with $Z \lesssim 0$, which implies a nonoptimal solution of CS. For accurate odor identification, the sparsity should be smaller than $K = 25$ [see Fig. 5(b) and Appendix A].

A. Odor identifiability varies across odorants with different functional groups

Odorants with certain functional groups, such as acids, terpenes, and aromatics, are characterized by Z scores with
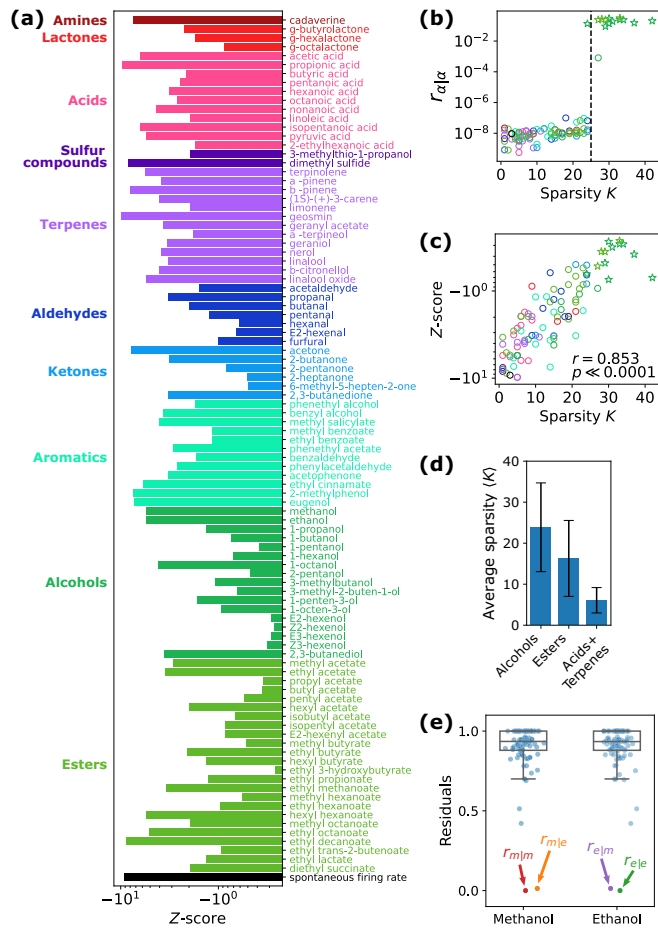
FIG. 5. Z score and sparsity K. (a) Z scores of the self-residuals for 96 odorants calculated from Fig. S3 [52]. (b) Self-residual $r_{\alpha|\alpha}$ versus the sparsity of $\mathbf{x}^{\mathrm{meas},\alpha}$. The odorants whose self-residual ($r_{\alpha|\alpha}$) is not minimal in the spectrum of residuals are marked with the star symbol. The black dashed line denotes the midpoint sparsity ($K = 25$) obtained by fitting the data to a logistic function. (c) Z scores of $r_{\alpha|\alpha}$ versus the sparsity (K) of $\mathbf{x}^{\mathrm{meas},\alpha}$. (d) The average sparsity of the odor response profile for odorants that displayed strong responses ($\geqslant 40$ spikes/s) under the specified functional group. (e) Distributions of the residuals for $\alpha = \mathrm{MeOH}$ and $\alpha = \mathrm{EtOH}$ ($r_{m|m} = r_{\mathrm{MeOH|MeOH}}$, $r_{m|e} = r_{\mathrm{MeOH|EtOH}}$, $r_{e|e} = r_{\mathrm{EtOH|EtOH}}$, and $r_{e|m} = r_{\mathrm{EtOH|MeOH}}$).

$Z \ll 0$ (Figs. S3 [52] and 5), implying that the uPN activation profiles for these odorants are unique at least among the odorants we tested, and hence the corresponding perceptual odor space can be unambiguously discerned from others. In contrast, alcohols and esters elicit stronger responses over many uPNs [54], resulting in $Z \lesssim 0$ [see Figs. 5(a) and S3 [52]]. The average sparsity ($\langle K \rangle$) of the activity profiles for alcohols and esters is greater than that of acids and terpenes combined by three- to fourfold [Fig. 5(d)]. The considerably high $\langle K \rangle$ of alcohols and esters are likely linked to their poor odor identifiability by the *Drosophila* olfactory system. This finding is consistent with a previous study suggesting that ORs encoding alcohols and esters are broadly tuned, while another set of ORs that encode acids and amines are narrowly tuned [55]. The relatively poor odor identifiability of alcohols and esters, revealed from our CS framework, might also be related to the fact that the information necessary to identify alcohols and esters is processed through channels other than MBONs. Specifically, stereotyped spatial segregation of fruit-odor encoding PNs has been observed [13], which leads to stereotyped connectivity to LHNs [16,56], suggestive of the existence of labeled lines [8,14,16,30,37,39]. The odor identification and the subsequent decision-making process for alcohols and esters may heavily rely on the coprocessing of information transmitted through both KCs and LHNs, as a sizable portion of LH projections converge with the downstream projection from MB calyx [8,31,57].

Still, esters such as ethyl methanoate and ethyl decanoate are well discernible in the perceptual space. The same holds for methanol and ethanol, except when compared to each other. The odor identifiability assessed from our CS framework suggests that *Drosophila* may not be able to tell the difference between methanol and ethanol [29], as the corresponding values of self- and cross-residuals are almost identical to each other [$r_{m|m} \approx r_{m|e}$ and $r_{e|e} \approx r_{e|m}$; see Fig. 5(e)].

B. Perceptual space of odor mixture and olfactory white

In natural environments, most odors originate from complex mixtures of odorants. In humans, it is known that exposure to multiple odorants leads to the loss of the odor characterization of individual components [58–60] and that a mixture consisting of an even greater number of odorants leads to a perceptual state called "olfactory white" [61]. This loss of odor differentiability is analogous to the loss in CS capacity, raising a question of how simultaneous exposure to multiple odorants affects our CS framework. To test this hypothesis, we examine our framework against (i) random mixtures of a predetermined number of odorants and (ii) natural odor mixtures of fruit extract.

When multiple odorants are randomly mixed, how does the brain perceive the odor? At the glomerular level, it has been suggested that an odorant mixture elicits glomerular activities [62] that may or may not be identical to the sum of the activities of individual glomeruli [63–65]. Competitive binding of odorants to receptors is expected [65–67] and some odorants may be more dominant than others depending on the chemical and perceptual composition of the mixture [53]. Here we try to assess the odor identifiability from the vector $\mathbf{x}^{\mathrm{meas},\alpha}$ encoding a natural odor whose precise chemical composition is unknown. First, we estimate the sparsity of the uPN activity profile associated with natural odors since the challenges encountered by the olfactory system translate to the difficulty of signal recovery via CS. We compare the results from single odorants and fruit extracts, the latter of which are available in the form of electrophysiological recordings on 23 glomeruli [29]. To make a fair comparison of fruit extracts against the mixture of single odorants, we analyze the responses to the single odorants using only 23 glomeruli, which are extended to the 47 uPNs, as in the actual measurement [see Fig. 6(a)]. The chemical composition of fruit odors is expected to be diverse and we observe a large variation in the sparsity among fruits. The sparsities of some fruits (e.g., banana) are high, to the point that their odor identifiability through CS is anticipated to be low. There is a chance that
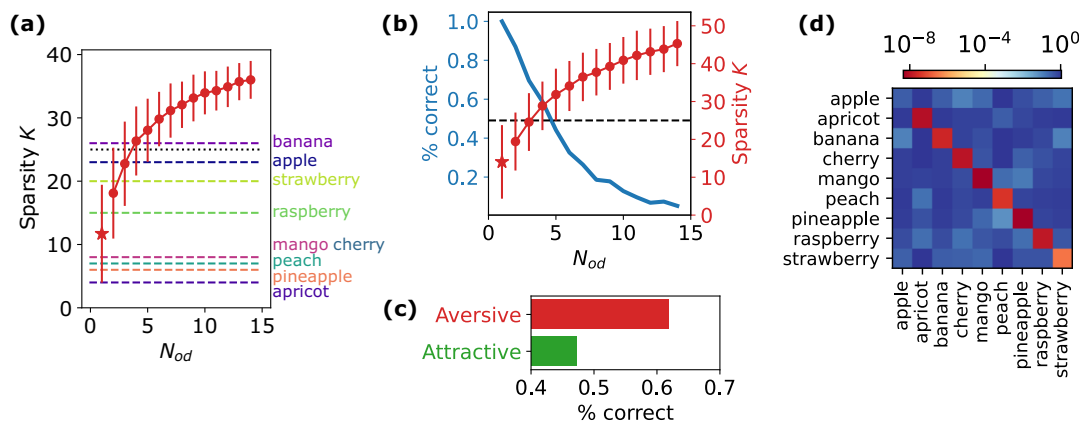
FIG. 6. Analysis of odor mixtures. (a) The average sparsity of randomly sampled odor mixture with different sample size N_{od} (red dots) and the sparsity of $\mathbf{x}^{\mathrm{meas},\alpha}$ when α = natural mixtures (dashed line). The sparsities are counted based on the 23 glomeruli whose responses were recorded in both the single odorant experiment and the fruit odor experiment for consistency. The red star denotes the average sparsity for single ($N_{od} = 1$) odorant exposure. The error bars indicate the standard deviation. The dotted black line corresponds to $K = 25$ in Fig. 5(b). (b) The input signal recovery (blue line) and the corresponding average sparsity (red dots) of a random mixture of odorants with different sample size N_{od}. The output is from the combined data set measuring 39 glomeruli against 83 odorants whose self-residual ($r_{\alpha|\alpha}$) was minimal. The red star denotes the average sparsity for single ($N_{od} = 1$) odorant exposure. The red error bar indicates the standard deviation. The dashed line corresponds to the midpoint sparsity ($K = 25$). (c) The probability of successful input signal recovery for the mixture consisting of two attractive odors (green) or two aversive odors (red). (d) The matrix of the residuals, $r_{\alpha|\beta}$, calculated based on fruit odors. Each row depicts the spectrum of the residuals of an odor input α with respect to other fruit odors β (β = apple, apricot, …) denoted in the horizontal axis.

the sparsity reported here is underestimated since other sets of glomeruli not recorded in the experiment may have activated. Furthermore, a natural odor, whose chemical composition is complex in reality, could display a small K when it is encoded by a small set of broadly tuned ORs [68].

For random odorant mixtures, we directly compared vectors $\hat{\mathbf{x}}$ and $\mathbf{x}^{\mathrm{meas}}$ to assess the accuracy of the signal recovery instead of calculating the residual spectra. Specifically, we assumed that the recovery was successful if the cosine distance between the two vectors, defined by $d_{\cos} = 1 - (\mathbf{x}^{\mathrm{meas}} \cdot \hat{\mathbf{x}})/(||\mathbf{x}^{\mathrm{meas}}||_2||\hat{\mathbf{x}}||_2)$, is smaller than 0.05. From the 83 odorants that the CS framework accurately identified, we randomly sampled the odorants to create 500 random mixtures with size N_{od}, linearly combined the uPN activity profiles of individual odorants in each mixture, and performed CS to infer $\hat{\mathbf{x}}$. As expected, we found that the chance of successful recovery of the original signal $\mathbf{x}^{\mathrm{meas}}$ declined as the number of odorants composing a mixture (N_{od}) increased, with the chance dropping below 20% for $N_{od} > 7$ (or $K > 40$) [Fig. 6(b)]. We note that mechanisms such as divisive normalization [69] and primacy coding [20] can increase the number of odorants in a mixture that linear, sparse coding-based CS can successfully recover. Yet, it still holds true that the performance of CS framework in the signal recovery gets less effective when many odorants are mixed at comparable concentrations.

However, the nature of the random odorant mixture can vary when the mixture is restricted to a specific valence. We select nine attractive odorants and seven aversive odorants, all of which are well characterized in terms of *Drosophila* behavioral response [8,16,36–39,70,71] (see Table S1) and create combinations of attractive or aversive odors by sampling two odorants from each category. We find that the capacity for signal recovery is significantly poor for the mixture of attractive odors compared to the mixture of aversive odors [Fig. 6(c)]. This may be associated with the generally poor odor

identifiability of alcohols and esters [Fig. 5(a)] that constitute many attractive odorants. While our result may not be directly translatable to the odor perception of *Drosophila in vivo*, the functional consequence of loss in the identifiability of an odor mixture is apparently analogous to the notion of "olfactory white."

In the case of natural mixtures (fruit extracts), we associated an activity profile for a fruit odor with a percept, such that α designates a type of fruit (e.g., apple). The measurements were made in response to the concentrated extracts from nine fruits (apple, apricot, banana, cherry, mango, peach, pineapple, raspberry, and strawberry) diluted to 10^{-2} volume per volume (v/v) with H_2O. Based on the results from random odorant mixtures, the recovery of activity from fruits such as apples and bananas whose uPN activity profile has high sparsity K does not seem guaranteed [Fig. 6(a)]. The spectrum of residuals is still specific enough to resolve the corresponding odors among a list of fruits except for apple, leading to a similar success rate as individual odors ($\sim$89%) and suggesting that their perceptual odor spaces in the brain of *Drosophila* are generally well separated [see Figs. 6(d) and S4 [52]].

C. Odor perception may depend on the odorant concentration

So far, our analysis has been conducted using electrophysiological recordings of odorants at a relatively high concentration. Both the recordings provided by Hallem and Carlson [29] and Seki *et al.* [30] employed 10^{-2} dilution with either H_2O, paraffin oil, or mineral oil (except for geosmin, which used 10^{-3} dilution) [30]. It is, however, known that the activity profile of ORNs and PNs are concentration dependent [22,29] and so is the observed hedonic valence of *Drosophila* to a given odorant [70,72]. Similar concentration-dependent behavioral responses have been observed in *C. elegans* [73].
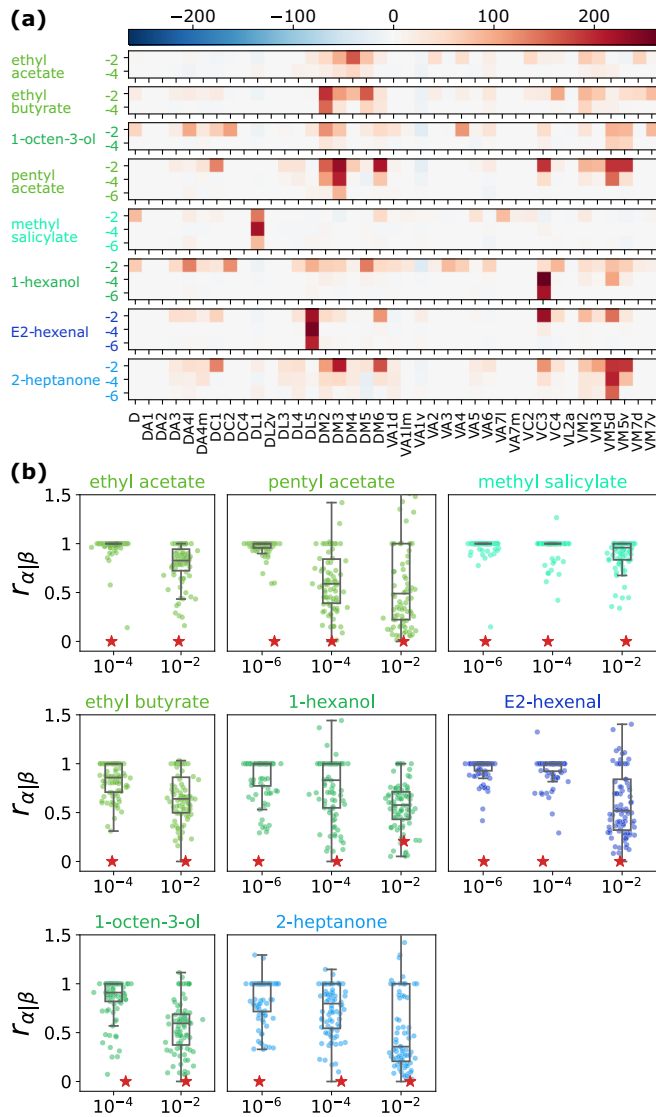
FIG. 7. Concentration-dependent perception of odor. (a) Electrophysiological recordings of uPN activity profiles in response to select odorants measured at different dilution levels (-2, -4, and -6 on the vertical axes signify the dilutions of 10^{-2}, 10^{-4}, and 10^{-6}, respectively). Only those that elicited a strong response to at least one homotype are plotted. (b) The distributions of $r_{\alpha|\beta}$ for odorants at different dilution levels. Red stars denote the self-residual $r_{\alpha|\alpha}$.

Figure 7(a) summarizes the electrophysiological responses of glomeruli to a small subset of odorants at varying dilution levels (10^{-8}, 10^{-6}, 10^{-4}, 10^{-2}) [29]. Some odorants evoke strong responses at low dilutions while others do not, which is consistent with the studies on odorant-dependent odor detection thresholds [66,74,75]. Odorants at unusually low concentrations may still be perceivable through a combination of specialized olfactory processing [76,77]; however, for consistency, we limit our study to dilution levels where there is an activation from at least a single neuron [see Figs. 7(a) and S5(a) [52]]. All eight odorants failed to evoke strong responses at 10^{-8} dilutions.

When performing CS, we included all the previously tested odorants, which were measured at 10^{-2} dilution while replacing the odorant α with different dilution levels. One odorant that evaded our CS framework at a high concentration, E2-hexenal, became identifiable at lower concentrations, exhibiting a minimal self-residual across cross-residuals [see Fig. 7(b)]. A significant reduction in the sparsity K at a lower odorant concentration [see Supplemental Material Fig. S5(a) [52]] helps CS accurately recover the uPN activity profile. Our finding also translates to natural mixtures. The high identifiability of fruit odor at 10^{-2} dilution drops significantly for undiluted fruit extracts [see Fig. S5(b) [52]].

Significant changes are observed for the residual spectra of the same odorant at different concentrations [see Fig. 7(b)]. For example, the residual distributions of pentyl acetate and E2-hexenal exhibit a drastic change from 10^{-6} to 10^{-4} and from 10^{-4} and 10^{-2} dilutions, respectively. Physiologically, a drastic shift in the residual distributions implies considerable changes in uPN activity and the corresponding MBON response profiles [see Fig. S5(c) [52]]. We surmise that this signifies an alteration of the odor percept in the perceptual space to the point that the odorant under two concentrations may be perceived as different odors. For ethyl butyrate, our calculation shows a concentration-dependent shift in the residual distribution, explaining the conflicting information on the *Drosophila* behavioral responses reported in the literature [8,70,78]. These results are reminiscent of the changes in the qualitative properties reported in human odor characterization experiments.

Lateral inhibition in PNs normalizes the PN responses and makes them closer, regardless of the odor concentrations [69], but this does not preserve sparsity. An odor under two vastly different concentrations can occupy disparate perceptual spaces, leading to a different odor percept, as the sparse encoding of odor to the receptor space is a prerequisite for odor identifiability under the CS framework.

V. DISCUSSION

The neurons and the synaptic connectivity associated with the *Drosophila* olfactory system are akin to the nodes and weight matrices of artificial neural networks (ANN). Whereas an ANN dynamically trains the weight matrix to gain functionality, our system operates on a preconfigured synaptic weight matrix. The synaptic characteristics observed from the *Drosophila* olfactory system, such as the seemingly randomized, *incoherent* synaptic interface between uPNs and KCs (Fig. S1 [52]) and the sparsity of uPN activity profiles (Fig. 3), are aligned well with the prerequisite for CS. Hence we have applied CS to the experimentally reconstructed physiological circuits of the *Drosophila* olfactory system to explore its capability of inferring the identity of the sensed odorant from its representation in the inner brain. By leveraging the relations of neural codes in the receptor space to the perceptual odor space represented by the MBON response profiles, we study the differentiability of an odor stimulus in the perceptual odor space and provide a conceptual explanation of perceptual phenomena such as olfactory white and concentration-dependent odor perception. Our study suggests that MBONs encode enough information for the fruit fly's brain to reconstruct the odor identity in addition to the odor valence.

As previous studies have acknowledged, whether or not CS is implemented in the *Drosophila* brain is unknown [21,79]. There is no direct evidence that the higher cortical area effectively leverages the randomization of the PN-KC interface and that there exists a necessary circuitry to perform l_1-norm minimization, although there are suggestions for the implementation of sparse coding in real organisms [50,80]. Nonetheless, it is fascinating to discover that the *Drosophila* olfactory system exhibits the structural prerequisites for CS. We hypothesize that, for the downstream neural circuitry beyond the odorant-OR interface, the compression of the information for chemical stimuli through the effectively randomized sensing matrix is beneficial for conserving signal integrity while reducing the bandwidth and resources necessary for signal transmission to the higher cortical area. It is also interesting to note that a randomly prewired network has shown to be more cost-effective with improved accuracy and network trainability in the recent computational development in ANN [81].

In the *Drosophila* olfactory system, additional components regulate the activities of PNs, KCs, and MBONs that are not explicitly included in our framework. The most notable are the peripheral interactions [65] present in the second- and third-order olfactory neurons. Lateral inhibitions by local neurons (LNs) [82] suppress the sensitivity of PNs to ORN inputs, thereby achieving gain control. With divisive normalization, the inhibitions scale with the total ORN activity [68,69], making it particularly relevant for odorant mixtures that activate similar ORNs [83]. Since lateral inhibition tends to sparsify the PN activity [69], our assessed identifiability for complex odor mixtures and highly concentrated odors may be the lower bound of the CS performance. KCs are also subjected to lateral inhibition through anterior paired lateral (APL) neuron that extensively innervates MB. APL takes input from KCs broadly and reciprocally inhibits KCs globally [84,85], denoising and sparsifying the KC activity. Finally, MBON responses are extensively modulated by DANs, which is the basis of associative learning and valence encoding [18,86]. While these neurons alter the activity of olfactory neurons, we report that their effects enhance the performance of our CS framework, generally improving the accuracy of CS and odor identifiability (see Appendixes F and G, Figs. 14 and 13). These results suggest that our original CS framework has been subjected to stringent conditions and the reported performance may be a conservative approximation.

In the olfactory system, both the synaptic transmission and the neuronal response to an odor are nonlinear [22,29,87,88] and a more sophisticated and physiologically correct model for the firing rate could be used [21]. However, the performance of CS-based odor identification is dominated by sparsity and is not significantly altered by the nonlinearity incorporated to the synaptic transmission. We test various nonlinear filters, such as a ReLU, a saddle-node on invariant cycle (SNIC) representing the input response between the firing rates of ORNs and PNs [89], or a sigmoidal response approximating the relationship between GCaMP signal and vesicle release [90]. We find the performance of CS by nonlinear filters comparable to that with a linear filter (see Fig. 11 and Appendix D). This, combined with our analyses on APLs

and DANs, indicates that a linear filter can still be efficacious in the framework of CS.

Noise filtration is implemented through inhibitory circuits composed of various antennal lobe LNs [69,91,92], GABAergic inhibitory PNs (iPNs) [15,56], DANs [17,18,86,93,94], and others. These regulatory circuits reduce noise and sparsify odor representation [28,82], both of which should improve the capacity of our CS framework. While we find that the 83 odorants maintain a respectable level of recovery even in the presence of a significant amount of noise (see Supplemental Material Fig. S6 [52]), the reduced noise can further sparsify the vector $\mathbf{x}^{\text{meas}}$ and ease the recovery and identification of the correct activity profile, especially for an odor mixture where a low sparsity of $\mathbf{x}^{\text{meas}}$ is not always guaranteed.

Lastly, the temporal dynamics of the signal, which has not been considered here, is critical for olfactory processing. For odor perception, time-varying changes in odor concentration play a pivotal role in odor identification, decision-making, and odor-guided navigation [20,95,96]. Other interesting psychophysical phenomena, such as olfactory fatigue (peripheral olfactory adaptation) [97], require temporal information to understand. Furthermore, the temporal dynamics are closely related to the primacy coding hypothesis, which predicts ORs that are activated earlier to govern the overall odor identity [20], thereby significantly reducing the difficulty of signal recovery at higher concentrations under our CS framework if implemented. Whereas we did not implement primacy coding due to the limitation in data, it may still be possible to infer the temporal characteristics from the concentration-dependent changes in the uPN activity profile as they highlight ORs most sensitive to a given odorant which should correlate with the order of activity. While we believe that the primacy coding is an effective principle behind concentration-invariant odor identification, we suspect that the less sensitive and therefore delayed ORN responses may also contribute to the odor perception as characterized by the concentration-dependent quality changes observed in humans.

In this work, we explored the concentration-dependent changes to projected perceptual space by entirely attributing it to the changes in the odor codes ($\mathbf{x}^{\text{meas}}$). Regarding the concentration-dependent valence, the aversion at high concentration is mediated by the signal through LH that defines the innate responses and the innate responses are in turn modulated by the output from MB calyx [30]. In light of classical conditioning experiments on *Drosophila* [98,99], which demonstrated the dramatic change in the *Drosophila* behavior in response to electric shock, it can be surmised that behavioral responses depend on both the multimodal sensory processes of odor identification and the learned responses. Modification in behavioral response (or decision making) may result from the multimodal integration of various sensory inputs not covered in this study.

Taken together, we demonstrate the capacity of the CS framework to recover high-dimensional uPN activity profiles from low-dimensional *barcodes* at MBONs in the *Drosophila* olfactory system. In fact, partial information on the MBON response profile still suffices to recover the corresponding uPN activity profile for many odorants (Appendix H), suggestive of much room for more efficient data compression and retrieval. It will still be of great interest to explore the

effects of incorporating the various neuronal features listed above into the basic structure of our CS framework.

All original data and codes are deposited and publicly available [100].

APPENDIX A: CONDITIONS FOR SOLVING THE INVERSE PROBLEM THROUGH COMPRESSED SENSING

We performed a detailed analysis of the synaptic connectivity between the layers of olfactory neurons to check whether it conforms to the criteria for successful recovery of the sparsest solution $\hat{x}$ through CS. Unlike the previous applications of CS to the olfactory system [21,26,27], where the true dimension of the odorant space is unknown, the dimensions of input and output vectors are well defined in our problem.

First, CS requires that the size of the input (m, the dimension of $\mathbf{b}$) be reasonably large compared to the dimension (n) and the sparsity (K) of the target vector to be recovered ($\mathbf{x}$). While the strict threshold for this criterion is often disputed [43,101], it has been demonstrated that m should be greater than the scale of $O(K \log(n/K))$ for a successful recovery of the $\hat{x}$ [101,102]. According to the synaptic connectivity provided by *Drosophila* hemibrain connectome [7], out of 162 uPNs, only 119 uPNs innervate MB calyx and connect to KCs [16]. These $n = 119$ uPNs that synapse with at least one of ~2000 KCs can be traced down to $m = 56$ MBONs based on the synaptic connectivity. Based on these numbers, and the typical sparsity of KCs in response to an odor, we believe that the dimensionality requirement of CS is generally satisfied.

We also approximated the incoherence criterion of the sensing matrix $\mathcal{A}$ constructed from two connectivity matrices, $\mathcal{C}^{\mathrm{PN-KC}}$ and $\mathcal{C}^{\mathrm{KC-MBON}}$, between uPNs, KCs, and MBONS. Traditionally, the coherence of a matrix $\mathcal{A}$ is defined through [103,104]

$$\mu = \max_{j,k, \ j \neq k} \mathcal{M}_{j,k}, \tag{A1}$$

where

$$\mathcal{M}_{j,k} = \frac{|\mathcal{A}_{,j} \cdot \mathcal{A}_{,k}|}{||\mathcal{A}_{,j}||_2 ||\mathcal{A}_{,k}||_2}. \tag{A2}$$

Here, $\mathcal{A}_{,i}$ denotes the ith column vector of $\mathcal{A}$. The value μ ranges from 0 to 1, with 0 indicating complete incoherence. Then, reconstructing a K-sparse vector $\hat{x}$ becomes highly probable under the following condition [104]:

$$K < \frac{1}{2}\left(1 + \frac{1}{\mu}\right). \tag{A3}$$

From the sensing matrix $\mathcal{A} = (\mathcal{C}^{\mathrm{PN-KC}} \cdot \mathcal{C}^{\mathrm{KC-MBON}})^{\mathsf{T}}$ and Eq. (A1), we obtain $\mu \approx 1$, which is the theoretical maximum. Based on this result, the reconstruction of the vector $\hat{x}$ through l_1-norm minimization seems infeasible. However, the requirement for incoherence, defined in Eq. (A1), is often
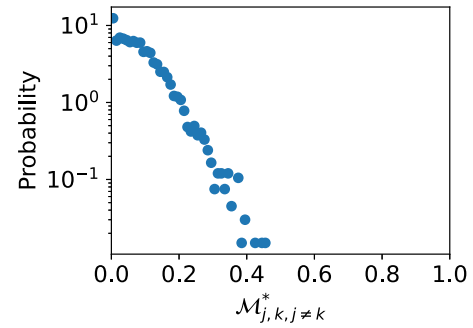

FIG. 8. Criteria required for successful signal recovery using the CS framework. The distribution of the pairwise correlation $\mathcal{M}^*_{j,k}$ between the connectivity matrices $\mathcal{C}^{\mathrm{PN-KC}}$ and $\mathcal{C}^{\mathrm{KC-MBON}}$.

considered unnecessarily stringent for CS, given that $\mu \sim 1$ is obtained even when a single pair of columns in the sensing matrix $\mathcal{A}$ are similar. As a result, several guidelines to relax the original criterion for incoherence have been suggested [103,105], requiring that the sensing matrix be only *effectively incoherent*.

In practice, it has been suggested that the recovery of a K-sparse vector is achievable with a high probability from asymptotically small μ as the size of $\mathcal{A}$ increases [104,105]. Brunton and Kutz have suggested a more relaxed condition [43]. When the sensing matrix $\mathcal{A}$ is a product of a measurement matrix $\mathcal{S}$ and a sparsifying basis Ψ, i.e., $\mathcal{A} = \mathcal{S}\Psi$, a small scalar product between the rows of $\mathcal{S}$ and the columns of Ψ is a good indication that l_1-norm minimization will recover $\hat{x}$, which replaces the matrix $\mathcal{M}_{j,k}$ [Eq. (A2)] with

$$\mathcal{M}^*_{j,k} = \frac{|\mathcal{S}_{j,} \cdot \Psi_{,k}|}{\|\mathcal{S}_{j,}\|_2 \|\Psi_{,k}\|_2}. \tag{A4}$$

While our $\mathcal{C}^{\mathrm{PN-KC}}$ and $\mathcal{C}^{\mathrm{KC-MBON}}$ are not analogous to the measurement matrix and the sparsifying basis by definition, the suggested requirement is mathematically equivalent within the scope of successful l_1-norm minimization subject to $\mathbf{b} = \mathcal{A}\mathbf{x}$. When we adopt $\mathcal{M}^*_{j,k}$ to approximate the incoherence criterion, a large portion of $\mathcal{M}^*_{j,k}$ are zero or close to zero (Fig. 8) and about 96% of the values are below 0.2, a theoretical limit that would allow CS to recover a target vector $\mathbf{x}$ with the sparsity of $K = 3$ [Eq. (A3)], which corresponds to an approximate average uPNs per glomerulus.

Restricted isometry property (RIP) is often cited as the rule of thumb when it comes to solving the inverse problem, but checking for RIP is often prohibitively expensive [104] and unnecessary in practical applications [105]. It has, indeed, been demonstrated that CS is possible even under weaker conditions [105,107]. We find that the sensing matrix of the *Drosophila* olfactory system is effective in recovering $\hat{x}$ for all practical purposes.

APPENDIX B: ASSESSING THE ODOR IDENTIFIABILITY BY MEANS OF RESIDUAL SPECTRUM

The specificity (identifiability or differentiability) of an odor α against other odors is assessed by evaluating the similarity between (i) the *measurement* and (ii) the *calculation* of the MBON response profile. (i) The measured MBON
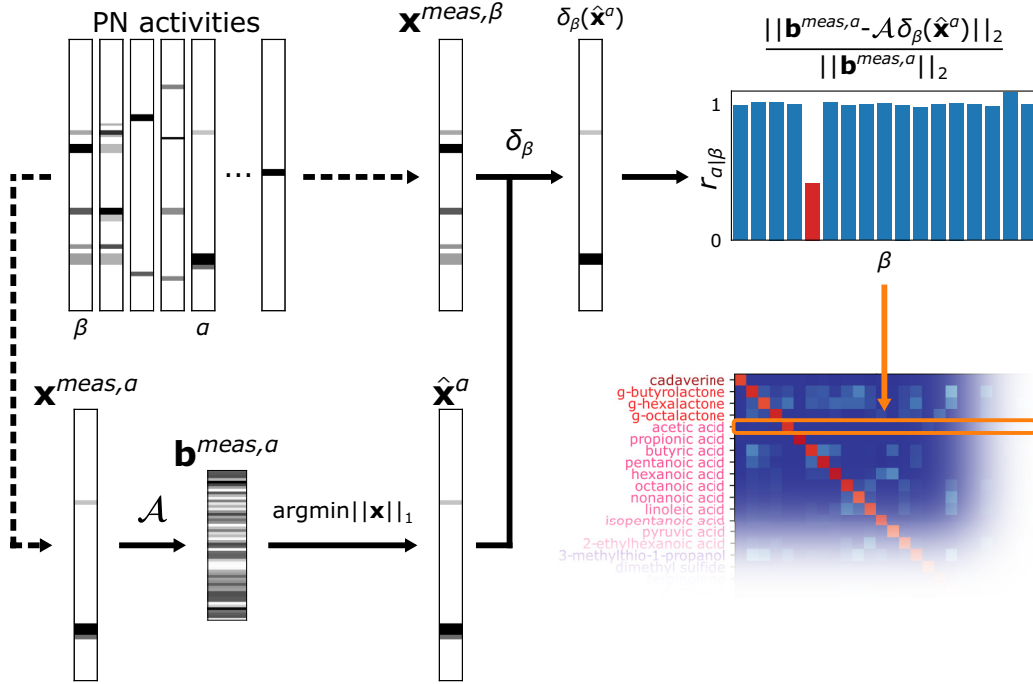
FIG. 9. Calculation of residual spectrum. uPN activity profile is used to calculate the input MBON response profile $\mathbf{b}^{\text{meas},\alpha}$, where α is an odorant. l_1-norm minimization is performed to determine the solution $\hat{\mathbf{x}}^\alpha$ from a set of underdetermined linear equations, which is compared with the input uPN activity profile $\delta_\beta(\hat{\mathbf{x}}^\alpha)$ filtered based on the expected uPN activity from another odorant β, $\mathbf{x}^{\text{meas},\beta}$. Adapting the framework of sparse representation for classification (SRC) [43,106], we calculate the residuals $r_{\alpha|\beta}$ for a given input odorant α and reference odorant β. The residuals for an odorant α against all other reference odorants $\{\beta\}$, $r_{\alpha|\beta}$ are calculated.

response profile, denoted by $\mathbf{b}^{\text{meas},\alpha}$, is acquired using the electrophysiological recording of uPN activity profile $\mathbf{x}^{\text{meas},\alpha}$ and the sensing matrix $\mathcal{A}$ via the relation $\mathbf{b}^{\text{meas},\alpha} = \mathcal{A}\mathbf{x}^{\text{meas},\alpha}$. (ii) A MBON response profile of the odor α can be calculated from $\mathbf{b}^\alpha = \mathcal{A}\hat{\mathbf{x}}^\alpha$ using the solution of the CS algorithm, i.e., $\hat{\mathbf{x}}^\alpha$ from Eq. (3).

To assess the differentiability of the odor α against other odors $\{\beta\}$, we adapted the sparse representation for classification (SRC) [43,106] and considered a function $\delta_\beta(\hat{\mathbf{x}}^\alpha)$ that filters the uPN activity profile calculated for the odor α against the uPN activity profile measured for the odor β. Specifically, the filtering function $\delta_\beta(\hat{\mathbf{x}}^\alpha)$ for the ith component of the uPN activity profile is defined as

$$[\delta_\beta(\hat{\mathbf{x}}^\alpha)]_i = \begin{cases} \hat{x}_i^\alpha, & x_i^{\text{meas},\beta} \neq 0, \\ 0, & x_i^{\text{meas},\beta} = 0. \end{cases} \quad \text{(B1)}$$

Note that the self-filtering yields the original profile, i.e., $\delta_\alpha(\hat{\mathbf{x}}^\alpha) = \hat{\mathbf{x}}^\alpha$. Along with Eq. (B1), we defined $r_{\alpha|\beta}$, the (relative) residual between the measurement ($\mathbf{b}^{\text{meas},\alpha}$) and the calculation $[\mathcal{A}\delta_\beta(\hat{\mathbf{x}}^\alpha)]$ over all test odors $\{\beta\}$ including $\beta = \alpha$, which enables us to assess the specificity of the odor α against all other odors $\{\beta\}$:

$$r_{\alpha|\beta} = \frac{\|\mathbf{b}^{\text{meas},\alpha} - \mathcal{A}\delta_\beta(\hat{\mathbf{x}}^\alpha)\|_2}{\|\mathbf{b}^{\text{meas},\alpha}\|_2}, \quad \text{(B2)}$$

where $\|\mathbf{x}\|_2 \equiv \sqrt{\sum_{i=1}^n x_i^2}$ (Fig. 9).

Ideally, $\mathcal{A}\delta_\alpha(\hat{\mathbf{x}}^\alpha)$ must be identical to $\mathbf{b}^{\text{meas},\alpha}$, i.e., $r_{\alpha|\alpha} = 0$, but, in practice, we find $r_{\alpha|\alpha} \gtrsim 0$. However, if $r_{\alpha|\alpha} \ll r_{\alpha|\beta}$ for all $\beta \neq \alpha$, then the odor represented by α can be

considered specific and easily discernible from other odors. In contrast, when there are many odors, say $\beta_1, \beta_2, \ldots$, satisfying $r_{\alpha|\alpha} \approx r_{\alpha|\beta_1} \approx r_{\alpha|\beta_2} \approx \cdots \approx r_{\alpha|\beta_k}$, it means that the odor space (perceptual space) of α is not well isolated from that of β, suggesting ambiguous sensing of odor α. In this case, discerning the odor α from other odors $\beta_1, \beta_2, \ldots, \beta_k$ is challenging for *Drosophila*.

To assess the spectrum of the residuals for the odor α, we calculated the Z score of $r_{\alpha|\alpha}$ defined as

$$Z = \frac{r_{\alpha|\alpha} - \mu_{r_{\alpha|\beta}}}{\sigma_{r_{\alpha|\beta}}}, \quad \text{(B3)}$$

where $\mu_{r_{\alpha|\beta}} = \frac{1}{N_\beta} \sum_\beta r_{\alpha|\beta}$ and $\sigma_{r_{\alpha|\beta}} = \frac{1}{N_\beta - 1} \sum_\beta (r_{\alpha|\beta} - \mu_{r_{\alpha|\beta}})^2$. Therefore, a Z score with $Z \ll 0$ implies that the value of the self-residual ($r_{\alpha|\alpha}$) is statistically well separated from the cross-residuals ($r_{\alpha|\beta}$) and the odor α is easily discernible from other odors.

APPENDIX C: ANALYSIS OF MBON RESPONSE PROFILES USING EUCLIDEAN DISTANCES

In this study, we utilize CS to discuss the differentiability between the MBON response profiles of various odorants. In principle, one could perform a similar analysis by calculating the distances between MBON response profiles. We, however, find that the results from such an analysis on high-dimensional vectors are often limited by the issues associated with the curse of dimensionality [50]. We find that the recovery of the
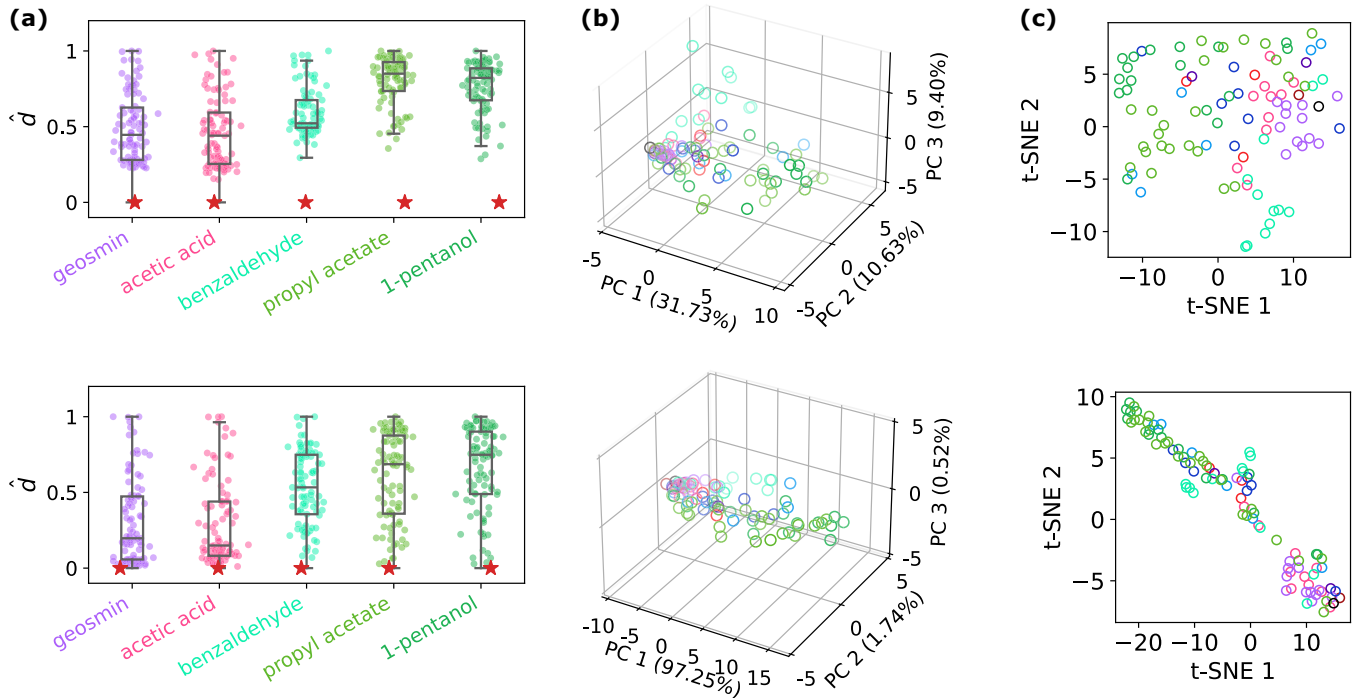
FIG. 10. Analysis of MBON response profiles using the Euclidean distances. (a) The distribution of scaled Euclidean distances between (top) uPN activity profiles and (bottom) MBON response profiles in response to select odorants. (b) The output of PCA projecting (top) uPN activity profiles and (bottom) MBON response profiles to three-dimensional space, along with the proportion of variance explained by each principal component. (c) The output of t-SNE projecting (top) uPN activity profiles and (bottom) MBON response profiles on two dimensions.

uPN activity through the CS algorithm is better suited for odor differentiability than other standardized methods.

Consider a pairwise distance matrix between MBON response profiles. Figure 10(a) shows the distribution of the scaled Euclidean distances between uPN activity profiles, $\hat{d}(\mathbf{x}^{\mathrm{meas},\alpha}, \mathbf{x}^{\mathrm{meas},\beta})$, where

$$\hat{d}(\mathbf{u}, \mathbf{v}) = d(\mathbf{u}, \mathbf{v}) / \max_{\mathbf{v}}[d(\mathbf{u}, \mathbf{v})], \tag{C1}$$

with $d(\mathbf{u}, \mathbf{v}) = [\sum_{i=1}^{n}(u_i - v_i)^2]^{1/2}$ and $\max_{\mathbf{v}}[d(\mathbf{u}, \mathbf{v})]$ being the maximum among the distances from the vector $\mathbf{u}$ to other vectors $\mathbf{v}$. The clear gap between the self- $[\hat{d}(\mathbf{x}^{\mathrm{meas},\alpha}, \mathbf{x}^{\mathrm{meas},\alpha}) = 0]$ and cross-distance $[\hat{d}(\mathbf{x}^{\mathrm{meas},\alpha}, \mathbf{x}^{\mathrm{meas},\beta}) > 0]$ found in the uPN activity profiles is no longer observable in the MBON response profiles $[\hat{d}(\mathbf{b}^{\mathrm{meas},\alpha}, \mathbf{b}^{\mathrm{meas},\beta})]$. This suggests that the Euclidean distance and its derivative measures are inadequate to characterize the highly integrated signal at MBONs [Fig. 10(a), bottom]. We observed a similar trend when we used other metrics such as cosine distance.

Incidentally, separation of the odor space by physiochemical features of odorants and OR/PN activities has previously been shown using principal component analysis (PCA) and t-distributed stochastic neighbor embedding (t-SNE) [22,29,70,71]. We performed PCA and t-SNE on a standardized matrix of MBON response profiles, in which each column of the matrix that represents MBON response profiles has zero mean and unit variance. PCA was performed using singular value decomposition (SVD) and t-SNE was performed using a perplexity of 15 after initializing with PCA.

The result of PCA indicates that, unlike uPN activity profiles, many odorants are hard to differentiate using MBON response profiles [Fig. 10(b)], where the proportion of variance explained by each principal component quickly diminishes after the first principal component [Fig. 10(b), bottom], suggestive of no clear separation in the odor representation. The lack of a clear separation in the component space is also found in the analysis using t-SNE [Fig. 10(c)].

APPENDIX D: TESTING NONLINEAR FILTERS FOR SYNAPTIC TRANSMISSION

Here we detail the three nonlinear filters (ReLU, SNIC, and sigmoid) that we used to reconstruct the sensing matrix and test the effect of nonlinear synaptic transmission. The ReLU filter is generated such that the synaptic weight under 8 is ignored—a criterion we used previously [16]. SNIC filter is generated based on the input-response relationship from the conductance-based Morris-Lecar type model [108]. Finally, a sigmoidal filter is generated according to [90], using 3 as the center point. We assumed that the strength of synaptic transduction directly correlates to the level of neurotransmitter release. For each nonlinear filter, the connectivity matrices ($\mathcal{C}^{\mathrm{PN-KC}}$ and $\mathcal{C}^{\mathrm{KC-MBON}}$) are passed through, which are then normalized, and the sensing matrix is constructed. We generated MBON responses from the newly formed sensing matrix and applied the CS framework to generate the corresponding residual spectra/Z scores. The correlation between the Z scores from the linear and the nonlinear models was evaluated
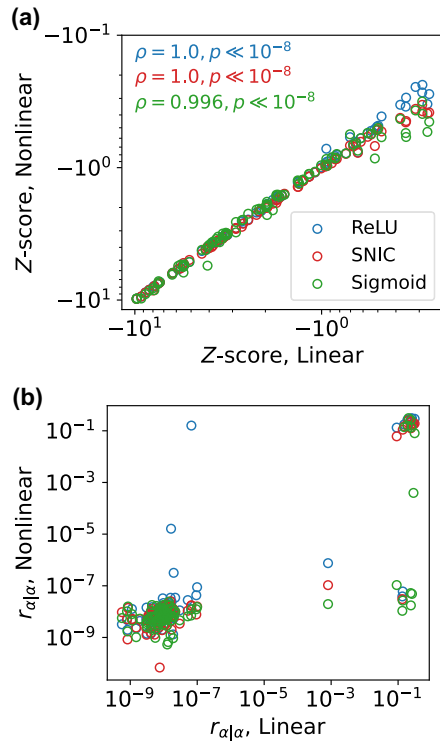
FIG. 11. Linear model well approximates the nonlinear models in CS. (a) Scatter plot between the Z scores of the self-residuals for 96 odorants under the linearity assumption and the Z scores after passing the connectivity matrices through a nonlinear filter. Three nonlinear filters, ReLU, SNIC, and sigmoid, are tested. Pearson correlation coefficient (ρ) and the corresponding p values are shown. (b) Scatter plot between the self-residuals $r_{\alpha|\alpha}$ under the linearity assumption and after passing the connectivity matrices through a nonlinear filter.

using the Pearson correlation coefficients and the corresponding p values [Fig. 11(a)].

APPENDIX E: COMPARING THE CS PERFORMANCE BETWEEN OBSERVED CONNECTIVITY AND RANDOM MATRICES

In applying CS, the sensing matrix is judiciously chosen to maximize the performance, where random matrices are considered the ideal choice [43]. Then, it is of great interest to ask how the observed connectivity in the *Drosophila* olfactory system compares to the random matrices. To compare the performance of CS, we tested three different randomized matrices, including sparse random, Bernoulli random, and Gaussian random matrices. The sparsities of random matrices are matched to the observed sparsity except for the Gaussian random matrix, which is naturally dense. To generate a Gaussian random matrix, we sampled from $\mathcal{N}(0, 1)$ with negative values set to zero. In addition to statistically random matrices, we tested a randomly shuffled version of the observed connectivity matrix. The performance across different matrices is assessed by comparing self-residuals $r_{\alpha|\alpha}$ and Z scores, as they measure how well CS recovered the sparsest vector $\hat{\mathbf{x}}$ and how differentiable the odor is, respectively.
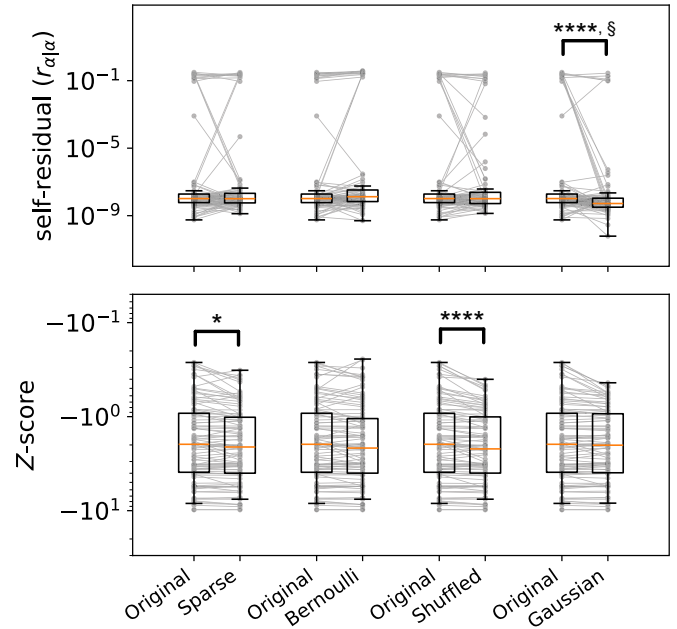

FIG. 12. Performance comparison between CS using the observed connectivity matrix and random matrices. Box plots of self-residuals $r_{(\alpha|\alpha)}$ and Z scores with the paired values for the 96 odorants are plotted. For most comparisons, the performance of CS using the observed connectivity matrix is not significantly different from that using random matrices. Original: the observed connectivity matrix. Sparse: sparse random matrix. Bernoulli: Bernoulli random matrix. Shuffled: randomly shuffled connectivity matrix. Gaussian: Gaussian random matrix. $*p < 0.05$, $****p < 10^{-4}$; Wilcoxon signed-rank test. $\S p < 10^{-3}$; Mann-Whitney U rank test.

We report that the observed connectivity matrices perform comparably to the randomized matrices (Fig. 12). Self-residuals $r_{\alpha|\alpha}$ were significantly smaller only for the Gaussian random matrix ($p < 10^{-4}$, Wilcoxon signed-rank test; $p < 10^{-3}$, Mann-Whitney U rank test). For odor differentiability, sparse random and shuffled observed matrices fared slightly better ($p < 0.05$ for sparse random; $p < 10^{-4}$ for shuffled, Wilcoxon signed-rank test; no significance in Mann-Whitney U rank test). For every other case, random matrices did not perform significantly better than the observed connectivity.

We emphasize that the significant improvement was achievable only when the KC-MBON connectivity was randomized. The observed connectivity between KCs and MBONs is far from random, as KCs and MBONs synapse within MB compartments [93,109]. However, given what is known about the innervation pattern of DANs, randomized connectivity between KCs and MBONs that removes the compartmentalized structure within MB will interfere with odor valence encoding and associative learning [86,93,110]. Therefore, we speculate that the observed connectivity balances the transmission of odor identity and olfactory learning.

APPENDIX F: TESTING THE LATERAL INHIBITION BY APL ON KCS

The APL neuron performs global inhibition in insect MB and sparsifies KC response through lateral inhibition [84].
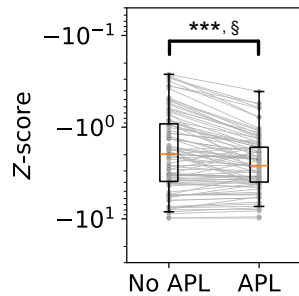
FIG. 13. Performance comparison between CS with (APL) and without (no APL) lateral inhibition by APL applied to the KC activity. Box plots of Z scores with the paired values for the 96 odorants are plotted. Z scores with lateral inhibition tend to be smaller, especially for odorants whose Z scores were large originally. $***p < 10^{-3}$; Wilcoxon signed-rank test. $\S p < 0.05$; Mann-Whitney U rank test.

To test the effect of the APL neuron on our CS framework, we collected all connections between APL and KCs from the hemibrain data set. Since KCs seem to recruit inhibition differentially and APL inhibits KCs with a similar strength [85], we devised a simple nonlinear model to approximate the KC activity when inhibition by APL is present ($\mathbf{KC}^*$), such that

$$\mathbf{KC}^* = \mathbf{KC} \cdot e^{-inh_{\mathrm{APL}}/\tau_{\mathrm{APL}}}, \tag{F1}$$

where

$$inh_{\mathrm{APL}} = \sum \frac{|\mathbf{KC}|}{\|\mathbf{KC}\|_2}. \tag{F2}$$

Here $\mathbf{KC}$ is a vector representing the KC activity and $\tau_{\mathrm{APL}} = 15$. Then, we computed the input MBON response profile $\mathbf{b}^{\mathrm{meas},\alpha}$ using $\mathbf{KC}^*$ without altering the sensing matrix and performed CS.

Figure 13 compares the Z scores for the same 96 odorants with and without lateral inhibition by APL applied to KCs. We see a significant decrease in Z scores when KC activity is further sparsified by lateral inhibition, indicating an increase in odor differentiability ($p < 10^{-3}$, Wilcoxon signed-rank test; $p < 0.05$, Mann-Whitney U rank test). The difference is particularly noticeable for odorants that had high Z scores originally, whose odor differentiability was relatively low. Overall, this result suggests that the wiring of the *Drosophila* olfactory system conforms to an effective CS and the real performance of CS may be better than what has been reported here.

APPENDIX G: TESTING THE DAN-BASED MODULATION OF KC-MBON CONNECTIVITY

When active and supplied with an odor in coincidence, DANs synapsing to KCs facilitate a long-term depression of the input to the unconditioned valence, consequently promoting MBONs with the opposite valence. While our framework cannot account for dynamic changes in the synaptic weight as seen in the learning process, olfactory learning tends to culminate in the modulation of the synaptic weight between KCs and MBONs by DANs. While olfactory learning is inherently multimodal, incorporating the olfactory signal and other sen-

sory information, connectomics data have shown that DANs often receive inputs from common upstream neurons, forming several DAN clusters [93]. We collected protocerebral anterior medial (PAM) and protocerebral posterior lateral 1 (PPL1) dopaminergic neurons that target KCs and categorized them based on previously identified 35 DAN clusters that received shared inputs [93]. For each DAN cluster, the synaptic weight between KCs and MBONs is altered according to the connectivity between DANs and KCs, from which the modified sensing matrix was computed, and the effect of the change was tested. Specifically, we defined the synaptic weight w between KCs and MBONs at steady state after conditioning as

$$w_i^* = \begin{cases} w_i^{KC}/w_j^{DAN} + \eta, & w_j^{DAN} > 0, \\ w_i^{KC}, & w_j^{DAN} = 0, \end{cases} \tag{G1}$$

for ith KC modulated by jth DANs before normalizing the connectivity matrix. To further diversify the synaptic strength, a Gaussian white noise $\eta(0, kw_i^{KC})$ with $k = 0.1$ was added since it was not possible to incorporate potentially synapse-specific, compartmentalized control of DANs on synapses between KCs and MBONs due to a lack of available data.

We found that the capacity of CS was effectively unaltered from the changes made in the KC-MBON connectivity (Fig. 14). On average, simulating the effect of depression by DANs increases the accuracy of CS slightly, with a generally higher recovery rate [Fig. 14(a)] and improved Z scores [Fig. 14(b)]. We hypothesize that the representation of an odor identity is preserved and independent of the modulation of synaptic connectivity by DANs and only the characteristic connectivity between PNs and KCs is necessary for the recovery of odor identity by the CS. Additionally, we note two other types of connections that may modulate the MBON response: (i) the feedback connections from MBONs to DANs or feedforward connections from KCs to DANs [17] and (ii) MBON-to-MBON interactions [93]. The consequence of these connections to the *Drosophila* odor identity and perception requires further studies.

APPENDIX H: ODOR IDENTIFICATION USING PARTIAL INFORMATION FROM MBONs

Our CS framework reconstructs the uPN activity from the response profile of 56 MBONs, where we assume that the MBON response profile reflects the information transmitted to the higher cortical area. Here, we consider a hypothetical situation where only partial information from the MBONs is available to the higher cortical area, perhaps due to some stereotyped connectivity, intrinsic stochasticity, and limited access to MBONs at a given time frame in animal perception, and ask whether the information encoded by a subset of MBONs is still enough to accurately infer the uPN activity profile [12]. For each of the 83 odorants our CS framework correctly identified, we randomly sample the MBON response profile 10 times with a sampling size N_{MBON} and examine whether at least one of the samples led to a correct identification. We find that a large number of odors can still be identified by using only a handful of MBONs, with the
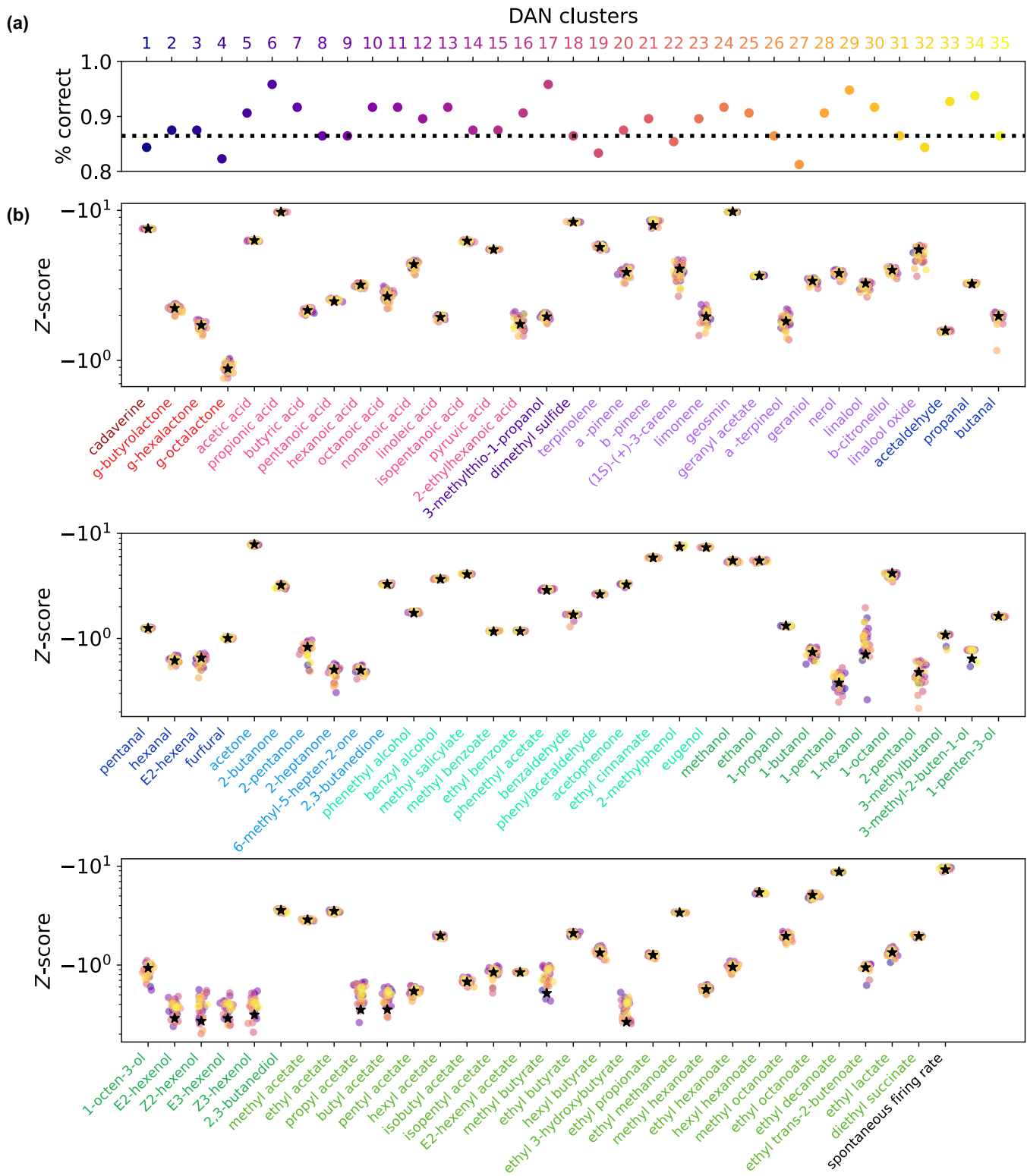
FIG. 14. Effect of DAN-based modulation on CS. (a) The percentage of signal recovery after applying DAN-based modulation. 35 DAN clusters with common input identified in [93] are used. The black dashed line denotes the success rate from the unaltered result. (b) *Z* scores of the self-residuals for 96 odorants after the application of DAN-based modulation. The results from applying 35 DAN clusters use the same color code in (a). Black stars denote *Z* scores from the unaltered result.
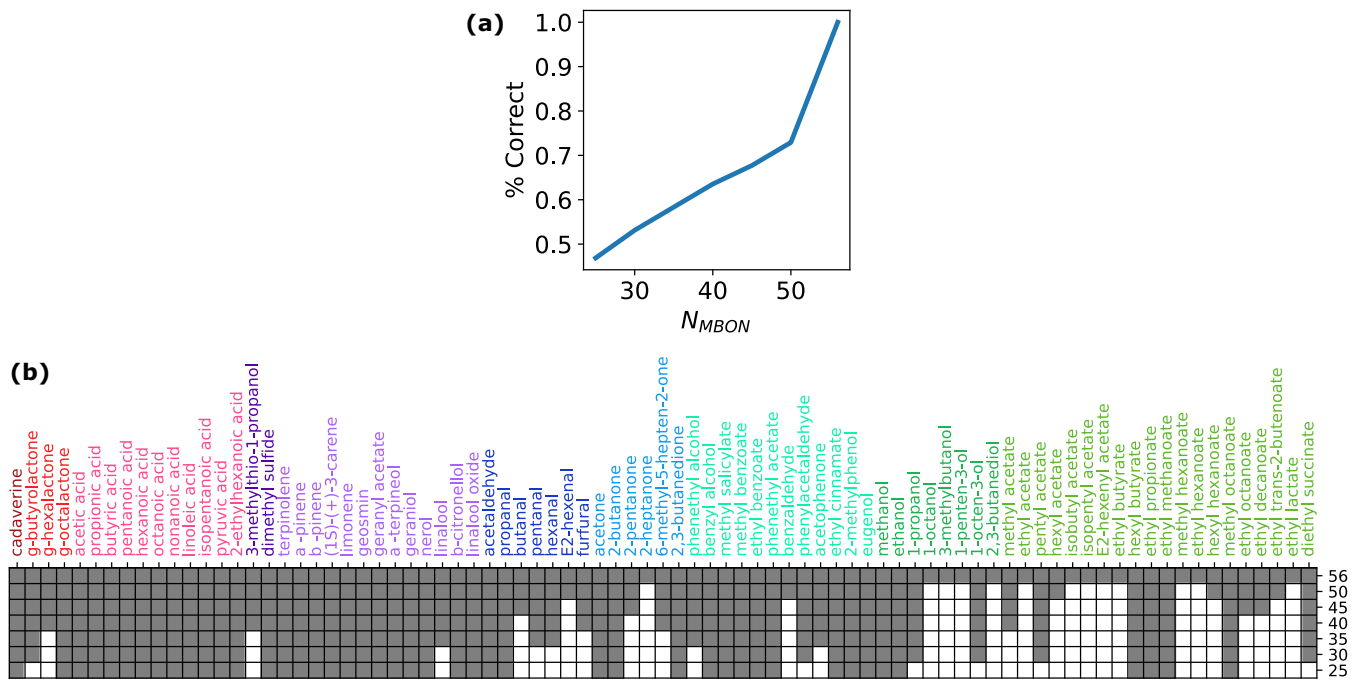
FIG. 15. Robustness of odor identification. (a) Testing the odor identifiability using a random subset of MBONs of the size N_{MBON}. The relationship between N_{MBON} and the success rate of odor identification. For a given odorant and a given size N_{MBON}, MBONs are sampled ten times, where the odor identification is considered successful if at least one set of the sampled MBONs can accurately identify the given olfactory stimulus. We employ the 83 odorants where the identification was successful in the original setup. (b) The results of the identification test on 83 odorants from a subset of MBONs with the size N_{MBON} labeled on the y axis. Gray denotes success and white denotes failure.

success rate improving with the sampling size N_{MBON} [see Fig. 15(a)]. We observe that the compressibility of information necessary to identify the odor varies with the functional group of the odorants. In particular, alcohols and esters are the first to fail as the size of N_{MBON} decreases [see Fig. 15(b)]. Odors from other functional groups (e.g., acids and terpenes) retain their accuracy even if the size of N_{MBON} is significantly small.

[1] C. Bushdid, M. O. Magnasco, L. B. Vosshall, and A. Keller, Humans can discriminate more than 1 trillion olfactory stimuli, Science **343**, 1370 (2014).

[2] R. C. Gerkin and J. B. Castro, The number of olfactory stimuli that humans can discriminate is still unknown, Elife **4**, e08127 (2015).

[3] M. Meister, On the dimensionality of odor space, Elife **4**, e07865 (2015).

[4] A. Koulakov, B. E. Kolterman, A. Enikolopov, and D. Rinberg, In search of the structure of human olfactory space, Front. Syst. Neurosci. **5**, 9271 (2011).

[5] Y. Zhou, B. H. Smith, and T. O. Sharpee, Hyperbolic geometry of the olfactory space, Sci. Adv. **4**, eaaq1458 (2018).

[6] D. Owald and S. Waddell, Olfactory learning skews mushroom body output pathways to steer behavioral choice in drosophila, Curr. Opin. Neurobiol. **35**, 178 (2015).

[7] L. K. Scheffer, C. S. Xu, M. Januszewski, Z. Lu, S.-y. Takemura, K. J. Hayworth, G. B. Huang, K. Shinomiya, J. Maitlin-Shepard, S. Berg *et al.*, A connectome and analysis of the adult *Drosophila* central brain, Elife **9**, e57443 (2020).

[8] A. S. Bates, P. Schlegel, R. J. Roberts, N. Drummond, I. F. Tamimi, R. Turnbull, X. Zhao, E. C. Marin, P. D. Popovici, S. Dhawan *et al.*, Complete connectomic reconstruction of

olfactory projection neurons in the fly brain, Curr. Biol. **30**, 3183 (2020).

[9] M. Winding, B. D. Pedigo, C. L. Barnes, H. G. Patsolic, Y. Park, T. Kazimiers, A. Fushiki, I. V. Andrade, A. Khandelwal, J. Valdes-Aleman *et al.*, The connectome of an insect brain, Science **379**, eadd9330 (2023).

[10] A. Couto, M. Alenius, and B. J. Dickson, Molecular, anatomical, and functional organization of the *Drosophila* olfactory system, Curr. Biol. **15**, 1535 (2005).

[11] S. J. Caron, V. Ruta, L. F. Abbott, and R. Axel, Random convergence of olfactory inputs in the *Drosophila* mushroom body, Nature (London) **497**, 113 (2013).

[12] C. F. Stevens, What the fly's nose tells the fly's brain, Proc. Natl. Acad. Sci. USA **112**, 9460 (2015).

[13] G. S. Jefferis, C. J. Potter, A. M. Chan, E. C. Marin, T. Rohlfing, C. R. Maurer, Jr., and L. Luo, Comprehensive maps of *Drosophila* higher olfactory centers: spatially segregated fruit and pheromone representation, Cell **128**, 1187 (2007).

[14] V. Ruta, S. R. Datta, M. L. Vasconcelos, J. Freeland, L. L. Looger, and R. Axel, A dimorphic pheromone circuit in *Drosophila* from sensory input to descending output, Nature (London) **468**, 686 (2010).

[15] L. Liang, Y. Li, C. J. Potter, O. Yizhar, K. Deisseroth, R. W. Tsien, and L. Luo, Gabaergic projection neurons route selective olfactory inputs to specific higher-order neurons, Neuron **79**, 917 (2013).

[16] K. Choi, W. K. Kim, and C. Hyeon, Olfactory responses of *Drosophila* are encoded in the organization of projection neurons, Elife **11**, e77748 (2022).

[17] C. Zhao, Y. F. Widmer, S. Diegelmann, M. A. Petrovici, S. G. Sprecher, and W. Senn, Predictive olfactory learning in *Drosophila*, Sci. Rep. **11**, 6795 (2021).

[18] A. Kato, K. Ohta, K. Okanoya, and H. Kazama, Dopaminergic neurons dynamically update sensory values during olfactory maneuver, Cell Rep. **42**, 113122 (2023).

[19] L. B. Vosshall, A. M. Wong, and R. Axel, An olfactory sensory map in the fly brain, Cell **102**, 147 (2000).

[20] C. D. Wilson, G. O. Serrano, A. A. Koulakov, and D. Rinberg, A primacy code for odor identity, Nat. Commun. **8**, 1477 (2017).

[21] N. Kadakia and T. Emonet, Front-end Weber-Fechner gain control enhances the fidelity of combinatorial odor coding, Elife **8**, e45293 (2019).

[22] G. Si, J. K. Kanwal, Y. Hu, C. J. Tabone, J. Baron, M. Berck, G. Vignoud, and A. D. Samuel, Structured odorant response patterns across a complete olfactory receptor neuron population, Neuron **101**, 950 (2019).

[23] S. Dasgupta, C. F. Stevens, and S. Navlakha, A neural algorithm for a fundamental computing problem, Science **358**, 793 (2017).

[24] S. Tootoonian and M. Lengyel, A dual algorithm for olfactory computation in the locust brain, Adv. Neural Inf. Process. Syst. **27** (2014).

[25] Y. Zhang and T. O. Sharpee, A Robust feedforward model of the olfactory system, PLoS Comput. Biol. **12**, e1004850 (2016).

[26] S. Qin, Q. Li, C. Tang, and Y. Tu, Optimal compressed sensing strategies for an array of nonlinear olfactory receptor neurons with and without spontaneous activity, Proc. Natl. Acad. Sci. USA **116**, 20286 (2019).

[27] K. Krishnamurthy, A. M. Hermundstad, T. Mora, A. M. Walczak, and V. Balasubramanian, Disorder and the neural representation of complex odors, Front. Comput. Neurosci. **16**, 917786 (2022).

[28] C. Dulac, Sparse encoding of natural scents, Neuron **50**, 816 (2006).

[29] E. A. Hallem and J. R. Carlson, Coding of odors by a receptor repertoire, Cell **125**, 143 (2006).

[30] Y. Seki, H. K. Dweck, J. Rybak, D. Wicher, S. Sachse, and B. S. Hansson, Olfactory coding from the periphery to higher brain centers in the *Drosophila* brain, BMC Biol. **15**, 56 (2017).

[31] P. Schlegel, A. S. Bates, T. Stürner, S. R. Jagannathan, N. Drummond, J. Hsu, L. S. Capdevila, A. Javier, E. C. Marin, A. Barth-Maron *et al.*, Information flow, cell types and stereotypy in a full olfactory connectome, Elife **10**, e66018 (2021).

[32] S. A. Ebrahim, H. K. Dweck, J. Stökl, J. E. Hofferberth, F. Trona, K. Weniger, J. Rybak, Y. Seki, M. C. Stensmyr, S. Sachse *et al.*, *Drosophila* avoids parasitoids by sensing their semiochemicals via a dedicated olfactory circuit, PLoS Biol. **13**, e1002318 (2015).

[33] V. Grabe, A. Baschwitz, H. K. Dweck, S. Lavista-Llanos, B. S. Hansson, and S. Sachse, Elucidating the neuronal architecture of olfactory glomeruli in the *Drosophila* antennal lobe, Cell Rep. **16**, 3401 (2016).

[34] K. E. Coates, A. T. Majot, X. Zhang, C. T. Michael, S. L. Spitzer, Q. Gaudry, and A. M. Dacks, Identified serotonergic modulatory neurons have heterogeneous synaptic connectivity within the olfactory system of *Drosophila*, J. Neurosci. **37**, 7318 (2017).

[35] T. T. Hayashi, A. J. MacKenzie, I. Ganguly, K. E. Ellis, H. M. Smihula, M. S. Jacob, A. Litwin-Kumar, and S. J. C. Caron, Mushroom body input connections form independently of sensory activity in *Drosophila* melanogaster, Curr. Biol. **32**, 4000 (2022).

[36] E. A. Hallem, M. G. Ho, and J. R. Carlson, The molecular basis of odor coding in the *Drosophila* antenna, Cell **117**, 965 (2004).

[37] C. G. Galizia and S. Sachse, *Odor Coding in Insect in The Neurobiology of olfaction*, edited by A. Menini (CRC Press, Boca Raton, 2009), pp. 35–70.

[38] S. Mansourian and M. C. Stensmyr, The chemical ecology of the fly, Curr. Opin. Neurobiol. **34**, 95 (2015).

[39] L. Badel, K. Ohta, Y. Tsuchimoto, and H. Kazama, Decoding of context-dependent olfactory behavior in *Drosophila*, Neuron **91**, 155 (2016).

[40] E. J. Candes, J. K. Romberg, and T. Tao, Stable signal recovery from incomplete and inaccurate measurements, Commun. Pure Appl. Math. **59**, 1207 (2006).

[41] D. L. Donoho, Compressed sensing, IEEE Trans. Inf. Theory **52**, 1289 (2006).

[42] C. E. Shannon, A mathematical theory of communication, Bell Syst. Tech. J. **27**, 379 (1948).

[43] S. L. Brunton and J. N. Kutz, *Data-driven Science and Engineering: Machine Learning, Dynamical Systems, and Control* (Cambridge University Press, Cambridge, UK, 2022).

[44] M. Lustig, D. Donoho, and J. M. Pauly, Sparse MRI: The application of compressed sensing for rapid MR imaging, Magn. Reson. Med. **58**, 1182 (2007).

[45] R. Leary, Z. Saghi, P. A. Midgley, and D. J. Holland, Compressed sensing electron tomography, Ultramicroscopy **131**, 70 (2013).

[46] J. B. Lee, A. Yonar, T. Hallacy, C.-H. Shen, J. Milloz, J. Srinivasan, A. Kocabas, and S. Ramanathan, A compressed sensing framework for efficient dissection of neural circuits, Nat. Methods **16**, 126 (2019).

[47] V. J. Barranca, G. Kovačič, D. Zhou, and D. Cai, Efficient image processing via compressive sensing of integrate-and-fire neuronal network dynamics, Neurocomputing **171**, 1313 (2016).

[48] P. C. Petrantonakis and P. Poirazi, A compressed sensing perspective of hippocampal function, Front. Syst. Neurosci. **8**, 141 (2014).

[49] B. Sun and W. Zhao, Compressed sensing of extracellular neurophysiology signals: A review, Front. Neurosci. **15**, 682063 (2021).

[50] S. Ganguli and H. Sompolinsky, Compressed sensing, sparsity, and dimensionality in neuronal information processing and data analysis, Annu. Rev. Neurosci. **35**, 485 (2012).

[51] V. J. Barranca, G. Kovačič, D. Zhou, and D. Cai, Sparsity and compressed coding in sensory systems, PLoS Comput. Biol. **10**, e1003793 (2014).

[52] See Supplemental Material at http://link.aps.org/supplemental/ 10.1103/PhysRevResearch.6.023298 for Table S1 and Figs. S1–S6.

[53] K. Shen, S. Tootoonian, and G. Laurent, Encoding of mixtures in a simple olfactory system, Neuron **80**, 1246 (2013).

[54] M. de Bruyne, K. Foster, and J. R. Carlson, Odor coding in the *Drosophila* antenna, Neuron **30**, 537 (2001).

[55] A. F. Silbering, R. Rytz, Y. Grosjean, L. Abuin, P. Ramdya, G. S. Jefferis, and R. Benton, Complementary function and integrated wiring of the evolutionarily distinct *Drosophila* olfactory subsystems, J. Neurosci. **31**, 13357 (2011).

[56] M. Fişek and R. I. Wilson, Stereotyped connectivity and computations in higher-order olfactory neurons, Nat. Neurosci. **17**, 280 (2014).

[57] M.-J. Dolan, S. Frechter, A. S. Bates, C. Dan, P. Huoviala, R. J. Roberts, P. Schlegel, S. Dhawan, R. Tabano, H. Dionne *et al.*, Neurogenetic dissection of the *Drosophila* lateral horn reveals major outputs, diverse behavioural functions, and interactions with the mushroom body, Elife **8**, e43079 (2019).

[58] D. G. Laing and G. Francis, The capacity of humans to identify odors in mixtures, Physiol. Behav. **46**, 809 (1989).

[59] D. Laing and B. Livermore, Perceptual analysis of complex chemical signals by humans, Chem. Signals Vertebrates **6**, 587 (1992).

[60] D. Poupon, P. Fernandez, S. Archambault Boisvert, C. Migneault-Bouchard, and J. Frasnelli, Can the identification of odorants within a mixture be trained? Chem. Senses **43**, 721 (2018).

[61] T. Weiss, K. Snitz, A. Yablonka, R. M. Khan, D. Gafsou, E. Schneidman, and N. Sobel, Perceptual convergence of multicomponent mixtures in olfaction implies an olfactory white, Proc. Natl. Acad. Sci. USA **109**, 19959 (2012).

[62] R. Tabor, E. Yaksi, J.-M. Weislogel, and R. W. Friedrich, Processing of odor mixtures in the zebrafish olfactory bulb, J. Neurosci. **24**, 6611 (2004).

[63] J. Joerges, A. Küttner, C. G. Galizia, and R. Menzel, Representations of odours and odour mixtures visualized in the honeybee brain, Nature (London) **387**, 285 (1997).

[64] N. Deisig, M. Giurfa, and J. C. Sandoz, Antennal lobe processing increases separability of odor mixture representations in the honeybee, J. Neurophys. **103**, 2185 (2010).

[65] T. Thomas-Danguin, C. Sinding, S. Romagny, F. El Mountassir, B. Atanasova, E. Le Berre, A.-M. Le Bon, and G. Coureaud, The perception of odor objects in everyday life: a review on the processing of odor mixtures, Front. Psychol. **5**, 504 (2014).

[66] J. H. Bak, S. J. Jang, and C. Hyeon, Implications for human odor sensing revealed from the statistics of odorant-receptor interactions, PLoS Comput. Biol. **14**, e1006175 (2018).

[67] W. K. Kim, K. Choi, C. Hyeon, and S. J. Jang, General chemical reaction network theory for olfactory sensing based on g-protein-coupled receptors: Elucidation of odorant mixture effects and agonist–synergist threshold, J. Phys. Chem. Lett. **14**, 8412 (2023).

[68] R. I. Wilson, Early olfactory processing in *Drosophila*: mechanisms and principles, Annu. Rev. Neurosci. **36**, 217 (2013).

[69] S. R. Olsen, V. Bhandawat, and R. I. Wilson, Divisive normalization in olfactory population codes, Neuron **66**, 287 (2010).

[70] M. Knaden, A. Strutz, J. Ahsan, S. Sachse, and B. S. Hansson, Spatial representation of odorant valence in an insect brain, Cell Rep. **1**, 392 (2012).

[71] S. D. Chakraborty, H. Chang, B. S. Hansson, and S. Sachse, Higher-order olfactory neurons in the lateral horn support odor valence and odor identity coding in *Drosophila*, Elife **11**, e74637 (2022).

[72] M. Ai, S. Min, Y. Grosjean, C. Leblanc, R. Bell, R. Benton, and G. S. Suh, Acid sensing by the *Drosophila* olfactory system, Nature (London) **468**, 691 (2010).

[73] K. Yoshida, T. Hirotsu, T. Tagawa, S. Oda, T. Wakabayashi, Y. Iino, and T. Ishihara, Odour concentration-dependent olfactory preference change in C. elegans, Nat. Commun. **3**, 739 (2012).

[74] S. Jang and C. Hyeon, Kinetic model for the activation of mammalian olfactory receptor, J. Phys. Chem. B **121**, 1304 (2017).

[75] C. Bontempi, L. Jacquot, and G. Brand, A study on the relationship between odor hedonic ratings and individual odor detection threshold, Sci. Rep. **12**, 18482 (2022).

[76] H. Kazama and R. I. Wilson, Homeostatic matching and nonlinear amplification at identified central synapses, Neuron **58**, 401 (2008).

[77] E. Perisse, C. Burke, W. Huetteroth, and S. Waddell, Shocking revelations and saccharin sweetness in the study of *Drosophila* olfactory memory, Curr. Biol. **23**, R752 (2013).

[78] D. MacWilliam, J. Kowalewski, A. Kumar, C. Pontrello, and A. Ray, Signaling mode of the broad-spectrum conserved CO_2 receptor is one of the important determinants of odor valence in *Drosophila*, Neuron **97**, 1153 (2018).

[79] C. Pehlevan, A. Genkin, and D. B. Chklovskii, A clustering neural network model of insect olfaction, in *2017 51st Asilomar Conference on Signals, Systems, and Computers* (IEEE, New York, 2017), pp. 593–600.

[80] A. A. Koulakov and D. Rinberg, Sparse incomplete representations: a potential role of olfactory granule cells, Neuron **72**, 124 (2011).

[81] P. Ghosal, S. Mahankali, and Y. Sun, Randomly initialized one-layer neural networks make data linearly separable, arXiv:2205.11716.

[82] A. F. Silbering and C. G. Galizia, Processing of odor mixtures in the *Drosophila* antennal lobe reveals both global inhibition and glomerulus-specific interactions, J. Neurosci. **27**, 11966 (2007).

[83] C. Linster and T. A. Cleland, Configurational and elemental odor mixture perception can arise from local inhibition, J. Comput. Neurosci. **16**, 39 (2004).

[84] M. Papadopoulou, S. Cassenaer, T. Nowotny, and G. Laurent, Normalization for sparse encoding of odors by a wide-field interneuron, Science **332**, 721 (2011).

[85] K. Inada, Y. Tsuchimoto, and H. Kazama, Origins of cell-typespecific olfactory processing in the *Drosophila* mushroom body circuit, Neuron **95**, 357 (2017).

[86] Y. Aso, D. Hattori, Y. Yu, R. M. Johnston, N. A. Iyer, T.-T. Ngo, H. Dionne, L. Abbott, R. Axel, H. Tanimoto *et al.*, The neuronal architecture of the mushroom body provides a logic for associative learning, elife **3**, e04577 (2014).

[87] R. D. Cazé, M. Humphries, and B. Gutkin, Passive dendrites enable single neurons to compute linearly non-separable functions, PLoS Comput. Biol. **9**, e1002867 (2013).

[88] A. Litwin-Kumar, K. D. Harris, R. Axel, H. Sompolinsky, and L. Abbott, Optimal degrees of synaptic connectivity, Neuron **93**, 1153 (2017).

[89] S. R. Olsen and R. I. Wilson, Lateral presynaptic inhibition mediates gain control in an olfactory circuit, Nature (London) **452**, 956 (2008).

[90] C. Schröder, J. Oesterle, P. Berens, T. Yoshimatsu, and T. Baden, Distinct synaptic transfer functions in same-type photoreceptors, Elife **10**, e67851 (2021).

[91] M. E. Berck, A. Khandelwal, L. Claus, L. Hernandez-Nunez, G. Si, C. J. Tabone, F. Li, J. W. Truman, R. D. Fetter, M. Louis *et al.*, The wiring diagram of a glomerular olfactory system, Elife **5**, e14859 (2016).

[92] A. A. Mohamed, T. Retzke, S. Das Chakraborty, B. Fabian, B. S. Hansson, M. Knaden, and S. Sachse, Odor mixtures of opposing valence unveil inter-glomerular crosstalk in the *Drosophila* antennal lobe, Nat. Commun. **10**, 1201 (2019).

[93] F. Li, J. W. Lindsey, E. C. Marin, N. Otto, M. Dreher, G. Dempsey, I. Stark, A. S. Bates, M. W. Pleijzier, P. Schlegel *et al.*, The connectome of the adult *Drosophila* mushroom body provides insights into function, Elife **9**, e62576 (2020).

[94] M. Adel and L. C. Griffith, The role of dopamine in associative learning in *Drosophila*: an updated unified model, Neurosci. Bull. **37**, 831 (2021).

[95] K. M. Cury and N. Uchida, Robust odor coding via inhalation-coupled transient activity in the mammalian olfactory bulb, Neuron **68**, 570 (2010).

[96] A. Parabucki, A. Bizer, G. Morris, A. E. Munoz, A. D. Bala, M. Smear, and R. Shusterman, Odor concentration change coding in the olfactory bulb, eNeuro **6**, ENEURO.0396-18.2019 (2019).

[97] P. Dalton, Psychophysical and behavioral characteristics of olfactory adaptation, Chem. Senses **25**, 487 (2000).

[98] W. G. Quinn, W. A. Harris, and S. Benzer, Conditioned behavior in *Drosophila* melanogaster, Proc. Natl. Acad. Sci. USA **71**, 708 (1974).

[99] T. Tully and W. G. Quinn, Classical conditioning and retention in normal and mutant *Drosophila* melanogaster, J. Comput. Phys. A **157**, 263 (1985).

[100] https://github.com/kirichoi/DrosophilaPerception.

[101] E. J. Candès, J. Romberg, and T. Tao, Robust uncertainty principles: Exact signal reconstruction from highly incomplete frequency information, IEEE Trans. Inf. Theory **52**, 489 (2006).

[102] E. J. Candes and T. Tao, Decoding by linear programming, IEEE Trans. Inf. Theory **51**, 4203 (2005).

[103] E. J. Candes, Y. C. Eldar, D. Needell, and P. Randall, Compressed sensing with coherent and redundant dictionaries, Appl. Comput. Harmonic Anal. **31**, 59 (2011).

[104] L. Stankovic, D. P. Mandic, M. Dakovic, and I. Kisil, Demystifying the coherence index in compressive sensing [lecture notes], IEEE Signal Process. Mag. **37**, 152 (2020).

[105] B. Adcock, A. C. Hansen, C. Poon, and B. Roman, Breaking the coherence barrier: A new theory for compressed sensing, in *Forum of Mathematics, Sigma* (Cambridge University Press, Cambridge, UK, 2017), Vol. 5, p. e4.

[106] J. Wright, A. Y. Yang, A. Ganesh, S. S. Sastry, and Y. Ma, Robust face recognition via sparse representation, IEEE Trans. Pattern Anal. Mach. Intell. **31**, 210 (2008).

[107] E. J. Candes and Y. Plan, A probabilistic and ripless theory of compressed sensing, IEEE Trans. Inf. Theory **57**, 7235 (2011).

[108] C. Morris and H. Lecar, Voltage oscillations in the barnacle giant muscle fiber, Biophys. J. **35**, 193 (1981).

[109] S.-y. Takemura, Y. Aso, T. Hige, A. Wong, Z. Lu, C. S. Xu, P. K. Rivlin, H. Hess, T. Zhao, T. Parag *et al.*, A connectome of a learning and memory center in the adult *Drosophila* brain, Elife **6**, e26975 (2017).

[110] Y. Aso and G. M. Rubin, Dopaminergic neurons write and update memories with cell-type-specific rules, Elife **5**, e16135 (2016).